https://doi.org/10.5194/egusphere-2024-3668
Preprint. Discussion started: 17 December 2024

Relict Landscape Evolution and Fault Reactivation in the Eastern Tianshan: Insights from the Harlik Mountains

Zihao Zhao[1], Tianyi Shen[2, *], Guocan Wang[1, 2, *], Peter van der Beek[3], Yabo Zhou[4], Cheng Ma[2]

[1]Institute of Geological Survey, China University of Geosciences, Wuhan, 430074, China
[2]Center for Global Tectonics, School of Earth Sciences, China University of Geosciences, Wuhan, 430074, China
[3]Institute of Geosciences, University of Potsdam, Potsdam, 14476, Germany
[4]PowerChina Huadong Engineering Corporation Limited, Hangzhou, 310012, China

Correspondence to: Tianyi Shen (shenty@cug.edu.cn) and Guocan Wang (wgcan@cug.edu.cn)

Abstract. Relict low-relief surfaces, formed during tectonically quiescent periods, are prevalent within the active mountain ranges of Central Asia, but the timing and processes of their formation within the Mesozoic-Cenozoic tectonic context remain poorly understood. In the Harlik Mountains of the easternmost Tianshan, extensive low-relief surfaces are preserved. Terrain analysis and structural interpretations based on DEM data reveal that these surfaces are segmented by WNW-ESE striking faults, which experienced an initial phase of right-lateral transtensional movement followed by left-lateral strike-slip reactivation. Apatite fission-track (AFT) thermochronology of samples from both relict surfaces and fault zones yields AFT ages ranging from ~110 to ~100 Ma for the relict surfaces, while samples from fault zones record ages of 90-70 Ma. Thermal modeling of these samples indicates a period of moderate cooling in the mid-late Early Cretaceous, followed by a prolonged slow cooling phase for the relict surfaces. In contrast, fault zones show rapid cooling during the 90-70 Ma interval. Integrating these data with previous findings, we suggest that the mid-late Early Cretaceous cooling event corresponds to extensional collapse following the Mongol-Okhotsk orogeny. This period of cooling, enhanced by humid climate conditions, likely promoted erosion and relief reduction, fostering the development of low-relief surfaces. Subsequently, the region experienced right-lateral transtensional faulting at 90-70 Ma, linked to continued extensional tectonics from the orogenic collapse. Late-Cretaceous faulting segmented the area without generating significant topographic contrasts across the relict surfaces. During the Oligocene (~30 Ma), far-field tectonic effects from the India-Eurasia collision initiated a new uplift phase that reactivated boundary and internal faults in a left-lateral sense. This phase marked the end of relief reduction, as surrounding basins began receiving sediments, and resulted in the uplift, dissection, and tilting of low-relief surfaces, ultimately contributing to the formation of the modern Eastern Tianshan Mountains.

1 Introduction

In orogenic belts worldwide, extensive high-elevation low-relief surfaces, typically forming summit plateaus or terraced pediments, bear testament to long-standing interactions between tectonic and surface processes (Phillips, 2002; Calvet et al., 2015; Whipple et al., 2017). These surfaces appear to be formed when erosion rates slow considerably, and their preservation is influenced by both tectonic stability and climatic conditions (van der Beek et al., 2009; Rohrmann et al., 2012; Morin et al., 2019). However, the processes behind their origin, preservation, and later modification remain a significant topic of debate. In particular, there is continued uncertainty regarding whether these low-relief surfaces developed at lower elevations and were subsequently uplifted during a phase of tectonic activity (Clark et al., 2006; Hetzel et al., 2011; Jaiswara et al., 2019) or whether they initially formed at high elevations within a tectonically uplifted environment (Liu-Zeng et al., 2008; van der Beek et al., 2009; Rohrmann et al., 2012; Cao et al., 2018). Understanding these processes offers insight into long-term landscape evolution, the timing and role of tectonic activity, and the response of landscapes to large-scale climatic fluctuations, all of which are vital for comprehending the evolution of mountainous terrains over geological timescales.

https://doi.org/10.5194/egusphere-2024-3668
Preprint. Discussion started: 17 December 2024

Central Asia, and particularly regions such as the Tianshan, Gobi-Altai, and western Mongolia, hosts an extensive array of such low-relief surfaces that have attracted considerable scientific interest due to their potential to reveal complex histories of tectonic and climatic interactions (**Fig. 1**; Jolivet et al., 2007, 2010; Gillespie et al., 2017a; Morin et al., 2019). These Central Asian relict surfaces are thought to reflect periods of tectonic stability following major Mesozoic to early Cenozoic tectonic events, with phases of tectonic activity including the Triassic-Early Jurassic, Late Jurassic-Early Cretaceous, and Late Cretaceous intervals (Jolivet et al., 2010, 2018; Gillespie et al., 2017a; Morin et al., 2019; He et al., 2021b). The tectonic history of the region is profoundly influenced by Mesozoic-early Cenozoic accretion-collision events along the southern Eurasian margin, commonly referred to as the Cimmerian collisions (Yin and Harrison, 2000; Kapp et al., 2007; Jolivet et al., 2010; Glorie and De Grave, 2016). These collisional events shaped the Tianshan region through cycles of uplift and erosion, leaving a lasting imprint on the landscape that includes the preservation of relict surfaces. Additionally, studies have suggested that the Mesozoic orogenic and subsequent collapse phases of the Mongol-Okhotsk tectonic belt may correlate with Mesozoic cooling episodes observed in the Tianshan Mountains (Gillespie et al., 2017a; Wang et al., 2018). The preservation of these relict surfaces since the Mesozoic provides critical constraints on the long-term tectonic, climatic, and surface processes that have shaped the Tianshan region (Jolivet et al., 2010, 2018; Glorie et al., 2011; Gillespie et al., 2017a; Jolivet, 2017; He et al., 2021b).

In the easternmost part of the Tianshan, the Harlik Mountain range (Harlik Shan or Qarliq Tagh) stands out as a unique region where high-elevation relict surfaces have been preserved along the southern slope. Thermochronological data suggest these surfaces may have formed during the Late Cretaceous to early Paleogene (Gillespie et al., 2017a; Chen et al., 2020b). This formation period likely corresponds to a phase of tectonic inactivity, when limited erosion allowed for the stabilization of these landscapes. Although it is generally agreed that late Cenozoic reactivation of bounding faults triggered the uplift of the Harlik Mountains, this phase of activity remains poorly constrained in terms of thermochronological data due to the minimal denudation associated with Cenozoic uplift (Cunningham et al., 2003; Gillespie et al., 2017a). Furthermore, previous research on the easternmost Tianshan's relict surfaces has typically involved sparse sampling confined to the periphery of the mountain range, leaving significant questions about the broader tectonic landscape evolution of this region unanswered.

Our study aims to bridge these gaps by thoroughly investigating the Harlik Mountains, focusing on the timing, formation processes, and subsequent deformation of its relict surfaces. Specifically, we integrate geomorphology, structural geology, and low-temperature thermochronology to unravel the complex interaction between tectonic processes and landscape development. Our approach includes digital terrain analysis to systematically extract and characterize relict surfaces in the Harlik Mountains. This analysis helps delineate the spatial distribution of relict surfaces, their preservation state, and the influence of local tectonic structures such as faults. Furthermore, we conduct a detailed structural analysis of the Harlik Mountains, with particular focus on the spatial relationship between regional faults and relict surfaces. Apatite fission track (AFT) dating, conducted on samples collected from several fragments of relict surfaces and key fault zones, serves as a critical tool for reconstructing the temporal relationship between surface formation, fault activity, and denudation. By analysing both the AFT data and geomorphological evidence, we establish a comprehensive temporal-spatial framework that allows us to contextualize the geomorphic and tectonic evolution of the Harlik Mountains in light of Mesozoic and Cenozoic tectonic activity.

https://doi.org/10.5194/egusphere-2024-3668
Preprint. Discussion started: 17 December 2024

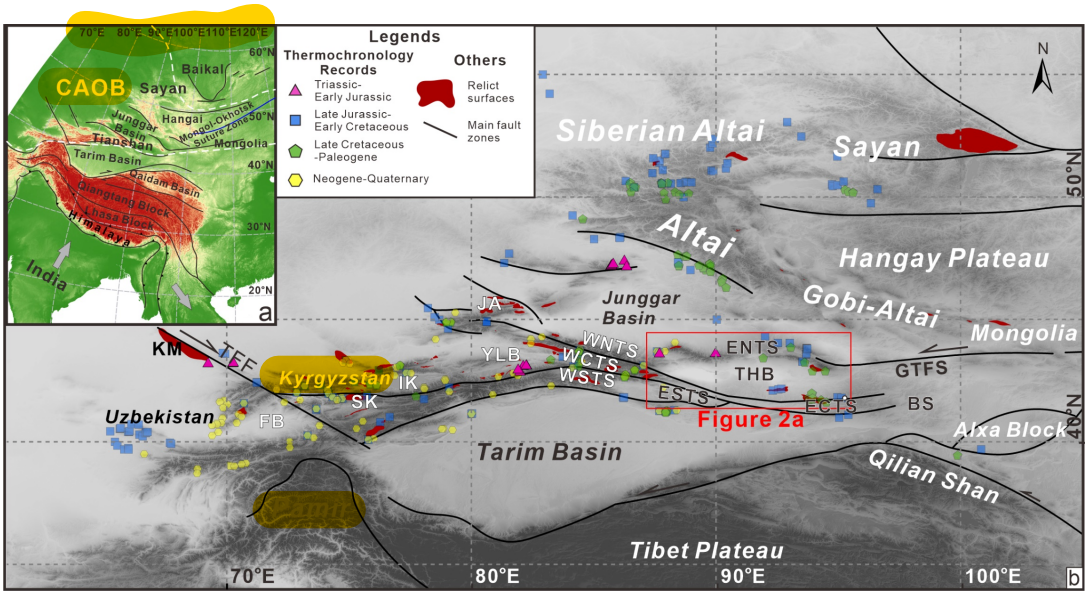

Figure 1: a. Tectonic sketch of the Central Asian Orogenic Belt (CAOB) and adjacent regions; b. Simplified topographic map of the Tianshan Orogenic Belt and adjacent areas, showing main tectonic units and faults. Rapid cooling episodes identified through thermochronology are marked, with data sourced from: De Grave and Van den haute (2002), Zhu et al. (2004, 2007), Shen et al. (2006), Sobel et al. (2006a, b), De Grave et al. (2007, 2008, 2014), Q. C. Wang et al. (2009), Zhang et al. (2009, 2011, 2016, 2021), Glorie et al. (2010, 2011, 2012a, b, 2019, 2023), Jolivet et al. (2010), Lu et al. (2013), Macaulay et al. (2014), Gao et al. (2014), Bande et al. (2015, 2017), De Pelsmaeker et al. (2015), Jia et al. (2015), Sun et al. (2015, 2021), Tang et al. (2015), Kassner et al. (2016), Tian et al. (2016), Gillespie et al. (2017a, b, 2021), Chen et al. (2018, 2020a, b), Jepson et al. (2018a, b, c, 2021b), Nachtergaele et al. (2018), Song et al. (2018), Wang et al. (2018), Yin et al. (2018), He et al. (2021b, 2022a, 2022b, 2023; 2024 in press), Zhimulev et al. (2021), Wu et al. (2023), and Jiang et al. (2024).

BS: Beishan; ECTS: Eastern Central Tianshan Mountains; ENTS: Eastern North Tianshan Mountains; ESTS: Eastern South Tianshan Mountains; FB: Fergana Basin; GTFS: Gobi-Tianshan fault system; IK: Issyk-Kul; JA: Junggar Alatau; KM: Karatau Mountains; SK: Song-Kul; TFF: Talas–Fergana fault; THB: Turpan-Hami Basin; WCTS: Western Central Tianshan Mountains; WNTS: Western North Tianshan Mountains; WSTS: Western South Tianshan Mountains; YLB: Yili Block.

2 Background

2.1 Geologic setting

The Tianshan Orogen, located along the southern margin of the Central Asian Orogenic Belt (CAOB; **Fig. 1**), comprises three main tectonic units: the northern, central, and southern Tianshan (Windley et al., 2007; Charvet et al., 2011; Xiao et al., 2013). The Tianshan has a complex geological history, initially marked by the accretionary collision of several microcontinents in the Paleozoic, followed by significant reworking due to strike-slip fault movement in the late Paleozoic (Windley et al., 1990, 2007; Xiao et al., 2013; He et al., 2021a). Subsequently, this region underwent several phases of intra-continental tectonic reactivation throughout the Mesozoic and Cenozoic (Windley et al., 1990; Dumitru et al., 2001). Notably, the southern Tianshan was subjected to significant compression and thrusting due to far-field stresses from the collision between the Indian and Eurasian plates, resulting in multiple large-scale tectonic deformation episodes (Bullen et al., 2001; Sobel et al., 2006a; Macaulay et al., 2014; Bande et al., 2015; Kassner et al., 2016).

Geographically, the Tianshan Belt is divided by the Urumqi-Korla line into western and eastern parts. The Western Tianshan is composed of the Western Chinese Tianshan and its extension into the Tianshan ranges of Kazakhstan, Kyrgyzstan, and

https://doi.org/10.5194/egusphere-2024-3668
Preprint. Discussion started: 17 December 2024

Uzbekistan (Figs. 1). The Eastern Tianshan, which encircles the Turpan-Hami Basin, includes the Moqinwula, Bogda-Barkol-Harlik, and Jueluotage Mountains from north to south (**Fig. 2**). The easternmost Tianshan forms part of the Harlik arc, a region that developed in response to the subduction of the Paleo-Asian Ocean and consists primarily of Ordovician-Carboniferous volcanic and volcaniclastic rocks (Xiao et al., 2004; Deng et al., 2016; Ji et al., 2019; Ni et al., 2021). In addition, Carboniferous and Permian igneous rocks are widespread in the easternmost Tianshan (Ma et al., 2015), with the Harlik Mountains dominated by Paleozoic strata and sizable granitoid and diorite plutons of mainly Silurian and Carboniferous age (**Fig. 2c**; Gillespie et al., 2017a; Ma et al., 2015).

The Harlik Mountains lie at the boundary between the northern Tianshan and the East Junggar arc or terrane, a location that has experienced multi-phase tectonic evolution during the Mesozoic and Cenozoic (Chen et al., 2020a). The Harlik Mountains are structurally linked to the Gobi-Tianshan fault system, a significant left-lateral strike-slip fault system that connects the eastern Tianshan with the Gobi-Altai. This fault system forms a restraining bend termination zone featuring a horsetail fault geometry (**Fig. 1**; Cunningham et al., 2003; Cunningham, 2013). The Harlik Mountains thus form an asymmetrical fault-bounded structure, delimited by the North Harlik Boundary Fault (NHBF), South Harlik Boundary Fault (SHBF), and Barkol Fault System (BFS) (**Fig. 2c**). This structure is marked by substantial uplift and denudation of the Paleozoic basement rocks to the north, while the southern slopes are capped by a gently dipping relict surface (Gillespie et al., 2017a).

Since the Mesozoic, tectonic activity in the easternmost Tianshan has been influenced by a range of tectonic settings, resulting in a complex structural system. During the Late Jurassic to Early Cretaceous, deformation transitioned from compression to extension, evidenced by Late Jurassic-Early Cretaceous folding and thrust faulting in the Moqinwula Mountains (Chen et al., 2020a) and mid- to late Early Cretaceous normal faulting in the Barkol Mountains (Chen et al., 2020b). Currently, tectonic activity in the Harlik Mountains remains closely associated with the far-field effects of the India-Asia collision, which has reactivated pre-existing fault systems and generated a characteristic southward-tilted structure (Cunningham et al., 2003; Gillespie et al., 2017a). The structural framework of the Harlik Mountains also reflects a regional transition in deformation style, from thrust-dominated deformation in the central Tianshan to transpressional deformation in the easternmost Tianshan, driven by the interaction between the rigid Tarim craton and the more deformable Junggar block (Cunningham et al., 2003; Cunningham and Zhang, 2021).

2.2 Mesozoic-Cenozoic evolution of relict surfaces in the Tianshan Mountains

In response to the Cenozoic India-Asia collision, individual ranges within the Tianshan were uplifted mainly along pre-existing faults, resulting in a basin-and-range type landform (Sobel et al., 2006a; Jolivet et al., 2010; Chen et al., 2018; Chang et al., 2019). Despite significant uplift, extensive low-relief surfaces—remnants of the Mesozoic to early Cenozoic topography—continue to be widely distributed throughout the Tianshan region (Jolivet et al., 2010, 2018; Morin et al., 2019; He et al., 2023). These surfaces provide evidence of multiple phases of erosion, tectonic stability, and subsequent reactivation. However, the processes underlying the development of these relict low-relief surfaces vary across different regions of the Tianshan.

2.2.1 Kazakh and Kyrgyz Tianshan

In Kazakhstan, southwest of the Talas-Fergana fault (**Fig. 1**), Allen et al. (2001) identified a tilted relict surface atop the Karatau Mountains. Although this surface has been dissected during the late Cenozoic, the age of its formation remains undetermined. In Kyrgyzstan, low-temperature thermochronology data indicate that high-altitude relict surfaces in the Issyk-Kul and Song-Kul areas were formed during a prolonged period of slow erosion, following a phase of significant exhumation in the Late Triassic to Early Jurassic (De Grave et al., 2011, 2013; Rolland et al., 2020). A sedimentary hiatus spanning the Middle Jurassic to Paleogene in surrounding basins, coupled with Neogene-Quaternary sediments partially covering these surfaces, suggests that they developed between the Jurassic and Paleogene (Burbank et al., 1999; De Pelsmaeker et al., 2018). However, limited apatite fission track thermochronology data imply that the Kyrgyz Tianshan experienced rapid exhumation

https://doi.org/10.5194/egusphere-2024-3668
Preprint. Discussion started: 17 December 2024

during the Cretaceous (Sobel et al., 2006a; De Grave et al., 2012; De Pelsmaeker et al., 2015). Chen et al. (2018) proposed that the low-relief surfaces in Kyrgyzstan emerged during a phase of tectonic stability between the Late Cretaceous and early Cenozoic.

2.2.2 Chinese Western Tianshan

The tectonic and geomorphic evolution of the Chinese Western Tianshan during the Meso-Cenozoic parallels that of the Kyrgyz Tianshan. In regions such as the Yili block, Western Central Tianshan, and Western South Tianshan, low-temperature thermochronology data indicate significant cooling during the Late Triassic to Early Jurassic, followed by slower cooling from the Middle Jurassic to Late Cretaceous (Jolivet et al., 2010; Wang et al., 2018; Glorie et al., 2019; He et al., 2021b, 2022b). The degree to which Late Jurassic to Early Cretaceous cooling influenced the Chinese Western Tianshan remains a topic of discussion (Dumitru et al., 2001; Jolivet et al., 2010; Wang et al., 2018; Glorie et al., 2019; Xiang et al., 2019). According to Jolivet et al. (2010), Wang et al. (2018), and He et al. (2021b), the Chinese Western Tianshan did not experience significant relief building during its Mesozoic evolution; instead, the low-relief surfaces were established during this period. A geomorphological and sedimentological investigation in the northern Chinese Western Tianshan (Jolivet et al., 2018) demonstrated that the Mesozoic relict surfaces transformed into multi-phased, nested erosional surfaces, which were subsequently incised by Late Cretaceous to early Paleogene paleo-valleys.

2.2.3 Eastern Tianshan

Recent studies have increasingly focused on the Eastern Tianshan, where relict surfaces and significant tectonic structures have been identified. Thermal-history modeling indicates that the primary cooling phase in the Jueluotage range occurred during the Triassic to Early Jurassic (Gong et al., 2021; Sun et al., 2021). This was followed by multiple cooling pulses recorded during the Early Cretaceous and Late Cretaceous-Paleogene (Gao et al., 2014; Sun et al., 2015, 2021; Gong et al., 2021; He et al., 2022a). Different datasets independently suggest a decrease in relief in the Jueluotage range during the Jurassic. Detrital zircon geochronology from the Turpan-Hami Basin reveals a significant decline in provenance linked to the Jueluotage range during the Middle to Late Jurassic (Shen et al., 2020; Qin et al., 2022). Both the Turpan-Hami Basin and parts of the Jueluotage range experienced burial during Jurassic deposition (Shao et al., 1999, 2003; Gong et al., 2021; Sun et al., 2021). The low relief and elevation of the Jueluotage range are presumably due to prolonged slow erosion during the Mesozoic and Cenozoic. Previous thermochronological studies of the Bogda Mountains have primarily concentrated on the western portion near Urumqi. AFT ages in the Bogda Mountains display a younging trend from southwest to northeast, reflecting progressive uplift and exhumation from the Late Jurassic to the Miocene (Tang et al., 2015). Thermal modeling has identified two rapid cooling events: one during the latest Jurassic to Early Cretaceous and another during the Oligocene to Miocene (Tang et al., 2015). An erosional surface (**Fig. 2a**) that intersects Paleozoic rocks in the Bogda Mountains is thought to have formed during a Mesozoic to Paleogene period of slow cooling between these two rapid cooling events (Tang et al., 2015; Morin et al., 2019; He et al., 2023).

In the easternmost Tianshan, most thermochronological data indicate cooling primarily during the Early to Middle Triassic, Early Cretaceous, and Late Cretaceous to Paleocene (Gillespie et al., 2017a; Chen et al., 2020a, 2020b; He et al., 2022a). Cunningham et al. (2003) documented a tilted low-relief surface preserved in the Harlik Mountains (**Fig. 2a**). Gillespie et al. (2017a) reported evidence of Late Cretaceous cooling through thermal history modeling of a sample collected from the edge of this surface, suggesting that the surface formed during the Late Cretaceous to early Paleogene and was subsequently tilted during the Cenozoic. Structural analysis and low-temperature thermochronology data indicate that the Moqinwula Mountains underwent two stages of deformation during the Late Jurassic and Late Cretaceous (Chen et al., 2020a). Chen et al. (2020a) proposed that the low-relief surfaces preserved on the summits of the Moqinwula Mountains were formed in the Early Cretaceous, situated between these two deformation stages.

https://doi.org/10.5194/egusphere-2024-3668
Preprint. Discussion started: 17 December 2024

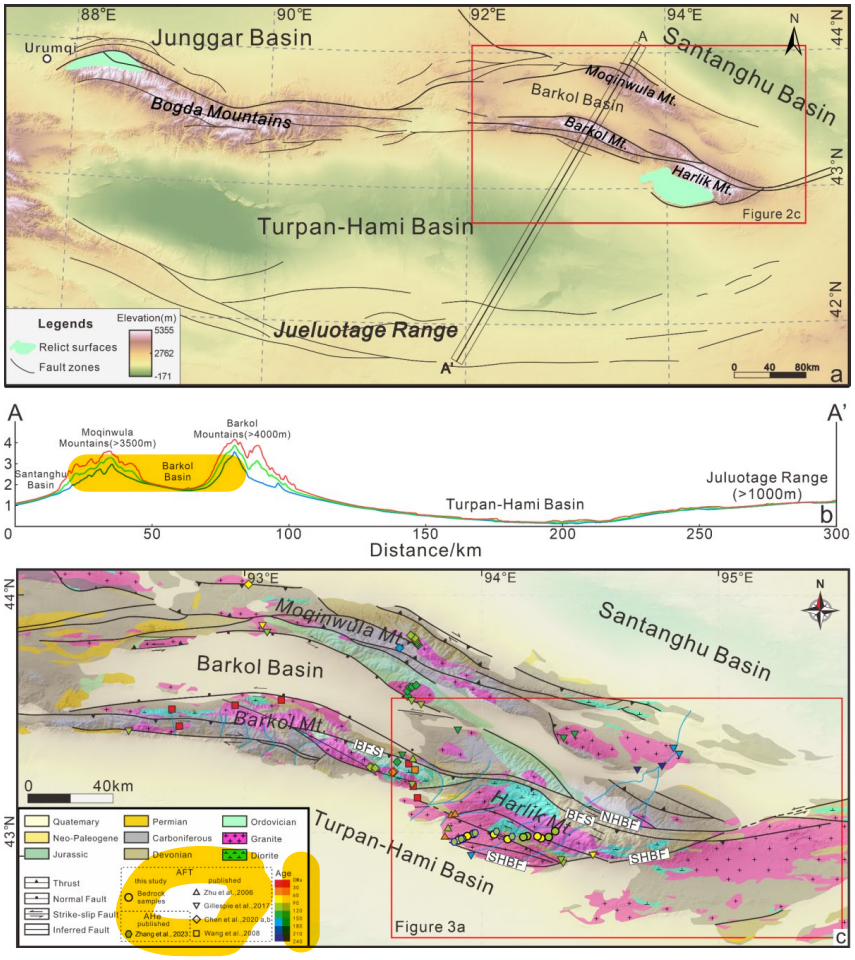

185 **Figure 2: a. Map showing the topography of the Eastern Tianshan and its main tectonic structures; b. topographic cross-section A-A' from the Santanghu Basin to the Jueluotage Range; c. Simplified geological map of the Easternmost Tianshan (modified from China Geological Survey, 2007)**

3 Tectonic Geomorphology

3.1 DEM-based terrain analysis

190 Although relict surfaces in the Harlik Mountains have been recognized for nearly two decades, studies have primarily focused on mapping and delineation using remote-sensing imagery and field surveys (Cunningham et al., 2003; Gillespie et al., 2017a). Morphologically, these surfaces are typically manifested as elevated positive relief landforms characterized by sub-horizontal or slightly tilted planar topography (Calvet et al., 2015; Yang et al., 2015a; Liu et al., 2019).

We employed digital terrain analysis based on the Shuttle Radar Topography Mission (SRTM) Digital Elevation Model (DEM),
195 which has a resolution of 3 arc seconds, to extract relict surfaces in the Harlik Mountains. Low-relief areas within and around the Harlik Mountains were delineated using a topographic slope criterion of less than 14° (Calvet et al., 2015; Haider et al., 2015; Liu et al., 2019). These areas encompass potential relict surfaces as well as low-relief regions in valleys and basins. To identify the relict surfaces within the mountain range, we excluded areas with a relative height of less than 40 m (**Fig. 3a**). The relative height is defined as the elevation difference between the original DEM and a reference erosion surface (Haider et al.,
200 2015). We extracted the drainage network from the DEM to identify river systems that have eroded the original low-relief

https://doi.org/10.5194/egusphere-2024-3668
Preprint. Discussion started: 17 December 2024

surfaces, using a threshold contributing area of 100 cells. An erosion reference surface was created by interpolating the elevations corresponding to the valley bottoms (i.e., the drainage lines). **Figure S1** provides a detailed description of the extraction procedure.

Based on the degree of preservation and the orientation of individual low-relief areas, we categorized the relict surfaces into several blocks (S1 to S9), as shown in **Fig. 3a**. To better understand the spatial relationships among the different relict surfaces, we extracted several NE-SW and NW-SE trending swath profiles (**Fig. 3b-f**). The NW-SE trending swath profiles reveal that elevations of the relict surfaces on the southern slope of the Harlik Mountains increase towards the east. Additionally, the relict surfaces in the eastern part of the range exhibit more pronounced erosion compared to those in the west (**Fig. 3b-d**). The NE-SW trending swath profiles illustrate significant topographic contrasts among these relict surfaces, with varying slopes dipping towards the south or southwest (**Fig. 3e-f**). Field observations indicate that these topographic contrasts are controlled by faults, which are discussed further in Section 3.2.

We extracted slope and aspect data for the grid points corresponding to the relict surfaces in different blocks, presented as slope-aspect rose diagrams (see **Figure S2**). The primary aspects of each surface are indicated with arrows in **Fig. 3a**. Some surfaces are represented by fan-shaped symbols, reflecting an angular range of aspects due to the absence of distinct individual aspects. The orientations of these surfaces are significantly influenced by boundary faults, including the North Harlik Boundary Fault (NHBF), the South Harlik Boundary Fault (SHBF), and the Barkol Fault System (BFS). Surface S1, bounded by the NHBF and BFS, features a gentle slope with a predominant westward aspect. Surface S3 is also bounded by the NHBF and BFS, gently dipping towards the northeast. Surface S2, located north of the NHBF, dips northeastward, perpendicular to the orientation of the NHBF. To the south of the BFS, surfaces S4, S5, and S7 predominantly dip towards the southwest. These surfaces are constrained to the north by the BFS and appear to be cut and variably tilted by different strands of the SHBF.

https://doi.org/10.5194/egusphere-2024-3668
Preprint. Discussion started: 17 December 2024

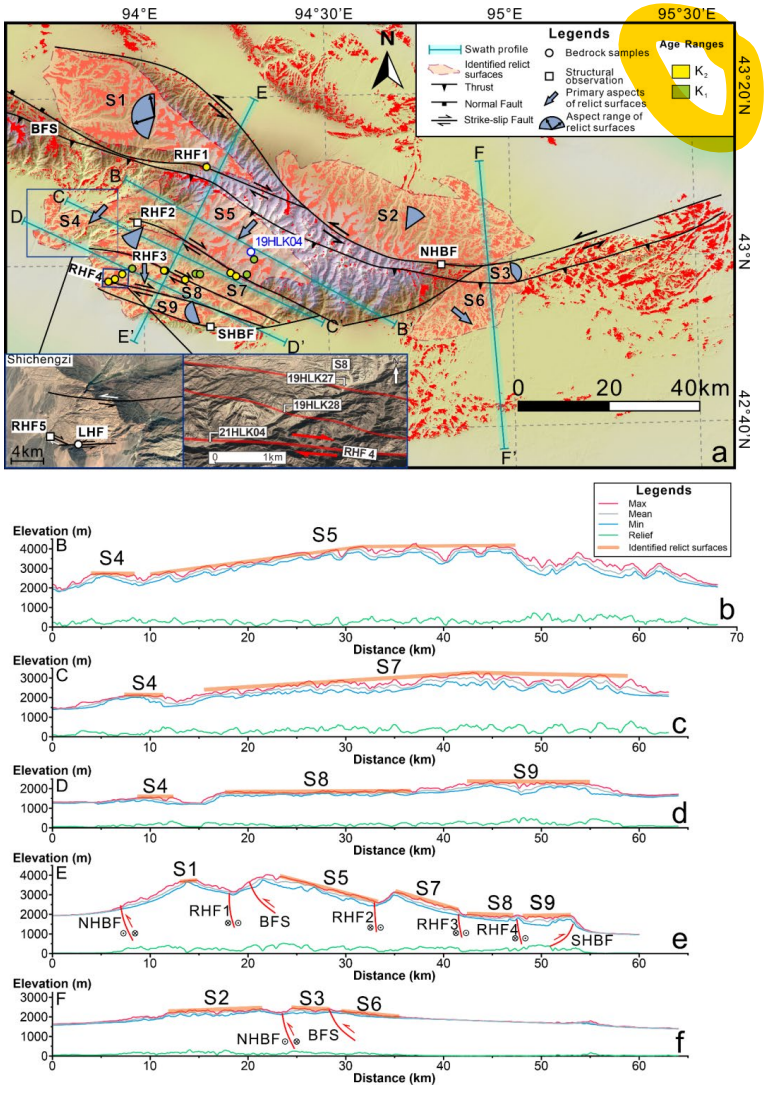

Figure 3: a. DEM of the Harlik Mountains with low-relief areas (slope <14°) in red; different identified relict surfaces are shown with pink shading and dashed outline. Insets show remote sensing imagery of Shichengzi area and RHF 4 in the lower left corner; b-f. topographic cross-sections B-B' to F-F' (see location in panel a)

3.2 Structural analysis

The relict surfaces in the Harlik Mountains are bounded by prominent topographic scarps visible on swath profiles, which correspond to linear boundaries in map view (**Fig. 3**). To better understand the formation and tectonic evolution of these surfaces, we conducted a detailed structural analysis of the Harlik fault system through field investigations.

The east-west trending NHBF delineates the northern edge of the Harlik Mountains. This fault exhibits a southward bend before extending eastward, where it merges with the Gobi-Tianshan fault (**Fig. 3a**). Field observations reveal that the NHBF displays predominantly left-lateral oblique strike-slip movement, with the southern block moving upward relative to the northern block. Slickenlines on the fault surface suggest a principal compressional stress direction oriented NE-SW (**Fig. 4a**). Similar to the NHBF, the SHBF also features low-angle thrust faults combined with high-angle left-lateral strike-slip faults (Figs. 4b-c).

https://doi.org/10.5194/egusphere-2024-3668
Preprint. Discussion started: 17 December 2024

Surface S1 is constrained by the NHBF to the north and by a right-lateral, NW-SE trending strike-slip fault (RHF 1) to the south (Figs. 3 and 4d). Additionally, three parallel NW-SE trending faults are present along the southern slope of the range, each demonstrating right-lateral strike-slip motion (Figs. 4e-g). These faults have fragmented the relict surfaces on the southern slope into separate blocks, each dipping southwestward at various angles. Paleo-stress analysis of RHF 2 and RHF 3 indicates NE-SW oriented extension, corresponding to the right-lateral movement along these faults (Figs. 4e-f). Field evidence also shows that ENE-WSW trending left-lateral strike-slip faults subsequently overprinted these NW-SE right-lateral faults. In samples collected from these strike-slip faults, hydrothermal features are evident, including veins of siliceous and carbonate fluids associated with fault activity, along with chloritization and epidotization alterations. These characteristics differ markedly from samples taken from the low-relief surfaces, suggesting localized fluid-rock interaction during fault activity (Figs. 4j-l).

In the Shichengzi area, located in the southwestern Harlik Mountains (**Fig. 3a**), we observed both NW-SE trending right-lateral strike-slip faults (RHF 5; **Fig. 4h**) and ENE-WSW trending left-lateral strike-slip faults (LHF; **Fig. 4i**). Remote-sensing imagery reveals that the LHF intersects RHF 5 (**Fig. 3a**), providing relative age constraints for these fault systems. Inferred stress tensors for these fault sets indicate NW-SE compression for RHF 5 (Fig. 4h) and NE-SW compression for LHF (**Fig. 4i**), further elucidating the complex, multi-phase deformation history of the Harlik fault system.

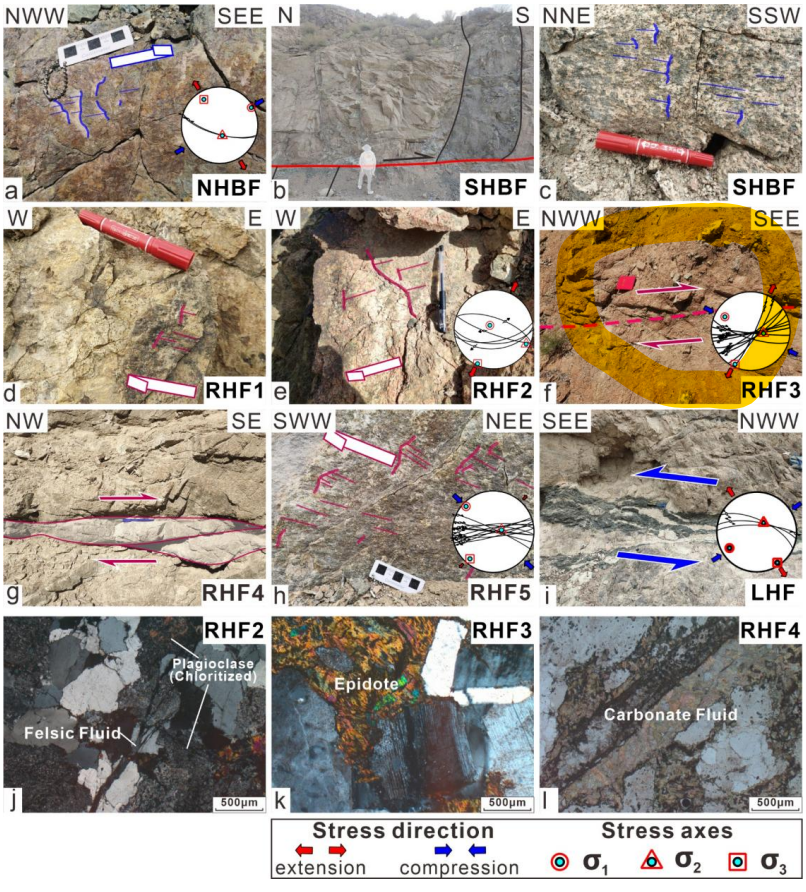

Figure 4: Outcrop photos of faults in the Harlik Mountains (locations of the study sites are shown in Fig. 3a). a. Slickenlines and steps on the NHBF fault surface indicate left-lateral oblique thrust motion, with corresponding paleo-stress orientations shown in the stereographic diagram. b. A low-angle thrust fault delineating the southern boundary of the Harlik Mountains, with movement indicated by offset veins. c. Slickenlines and steps on the SHBF fault surface, reflecting left-lateral movement. d. Slickenlines and steps on the RHF 1 fault surface, indicative of right-lateral movement. e. Slickenlines and steps on the RHF 2 fault surface, also

https://doi.org/10.5194/egusphere-2024-3668
Preprint. Discussion started: 17 December 2024

indicating right-lateral movement, with corresponding inferred paleo-stress orientations; f. En-echelon cracks on RHF 3, demonstrating right-lateral motion, along with corresponding paleo-stress orientations. g. Asymmetric granitic lenses indicative of dextral shear along the RHF 4. h. Slickenlines and steps on the RHF 5 fault surface, showing dextral movement and corresponding paleo-stress orientations. i. σ-shaped granitic lenses indicating a sinistral sense of ductile shear along the LHF, with paleo-stress orientations revealed by fault data from the brittle segments of the same fault. j. Chloritization of plagioclase and siliceous fluid vein observed in the RHF 2. k. Epidote alteration in RHF 3. l. Carbonate fluid vein in RHF 4.

4 Low-temperature thermochronology

Low-temperature thermochronology was employed to elucidate the evolutionary history of low-relief surfaces in the Harlik Mountains. This technique serves as a valuable tool for constraining both the magnitude and timing of denudation, as fluctuations in denudation rates are often correlated with the formation, preservation, and degradation of low-relief surfaces in mountainous regions (e.g., van der Beek et al., 2009; Rohrmann et al., 2012; Morin et al., 2019; Cao et al., 2022). Typically, tectonic activity can cause rapid exhumation, leading to relief development and fast cooling. As tectonic activity decreases, erosion lowers the relief, resulting in a period of slow cooling linked to low denudation. A phase of thermal stability, with no significant vertical movements, corresponds to low-relief topography, until tectonic reactivation leads to renewed uplift and exhumation. In the Harlik Mountains, relict surfaces are fragmented into several blocks by faults and incised valleys, indicating a complex history of relief rejuvenation. Thus, rocks situated on these relict surfaces are expected to preserve cooling histories reflective of both relief-building and subsequent leveling processes, while those located near faults or within valleys may record late-stage cooling events linked to relief rejuvenation (e.g., Cao et al., 2022).

4.1 Sampling strategy

While previous studies have reported low-temperature thermochronology data from the Harlik Mountains, the majority of these data have been collected from the margins of the mountain belt or the main valleys within the mountains (Zhu et al., 2006; Gillespie et al., 2017a; He et al., 2022a; Zhang et al., 2023). Consequently, the relationship between these samples and the relict surfaces or fault systems remains ambiguous. To investigate the relief evolution in the Harlik Mountains, we systematically collected samples for low-temperature thermochronology along two valleys situated on the southern slope of the mountain range. The samples encompass the four main identified blocks and the fault zones dividing them. Sampling was conducted at an average elevation interval of 200-300 m, ranging from 1155 m to 3747 m (**Table 1**). A detailed description of the samples, including their geographic locations and AFT age data, is provided in **Table 1**.

Table 1

Location	Sample Information					Ages								Track lengths			Mean D_{par} (μm)
	No.	Location			Lith.	n	ρ_s (10^5 cm^{-2})	N_s	^{238}U (ppm)	Pooled age (Ma± 1σ)	P(χ^2) (%)	Dispersion (%)	Central age (Ma± 1σ)	MTL (μm)	SD (μm)	N	
		Lon.	Lat.	Ele. (m)													
RHF 1 fault zone	**23HLK02**	94.175	43.194	2783	Granite	**25**	6.87	553	15.63	89.9±4.8	9.1	14	90.7±4.8	12.9	1.2	100	2.5
S5	**19HLK01**	94.280	42.979	3390	Granite	**15**	4.33	156	8.03	108.5±4.8	100	0	109.6±8.4	12.5	2.1	35	1.1
	19HLK02	94.300	43.009	3747	Granite	**16**	6.98	454	12.93	101.6±2.8	100	0	102.1±6.0	12.4	1.5	105	1.2
RHF 2 fault zone	**19HLK07**	94.249	42.974	3097	Diorite	**18**	18.46	660	52.98	70.2±4.6	2.8	15	73.1±4.0	12.1	1.2	140	1.5
	19HLK08	94.235	42.982	2799	Diorite	**18**	12.21	643	29.38	83.5±4.9	33	7	85.6±4.7	12.4	1.2	82	1.5
	19HLK10	94.197	42.986	2474	Granite	**20**	5.71	336	13.43	84.1±4.6	90	15	86.0±5.5	12.6	1.2	61	1.2
S7	**19HLK14**	94.152	42.981	2152	Granite	**17**	5.37	369	9.97	110.1±2.8	100	0	110.6±6.5	12.8	1.3	58	1.4
	19HLK15	94.141	42.982	2026	Granite	**18**	6.06	335	10.96	105.9±4.4	97	17	107.4±7.0	12.5	1.6	26	1.4
RHF 3 fault zone	**19HLK17**	94.112	42.970	1849	Diorite	**15**	5.78	295	14.82	76.5±4.5	96	0	77.7±5.6	12.1	1.2	35	1.4
	19HLK22	94.058	42.989	1847	Granite	**19**	6.35	260	18.96	80.2±5.4	55	0	80.1±4.8	12.4	1.2	28	1.4
	19HLK24	94.055	42.989	1869	Granite	**17**	8.75	236	20.69	74.0±4.2	91	0	75.6±5.5	12.9	0.9	18	1.5
S8	**19HLK26**	93.968	42.993	1619	Granite	**15**	3.66	201	8.92	102.4±3.4	100	0	103.1±8.0	12.0	1.4	43	1.2
	19HLK27	93.941	42.983	1516	Granite	**13**	8.42	276	21.57	69.8±6.3	75	19	72.4±6.4	12.6	1.2	50	1.2
	19HLK28	93.921	42.973	1398	Granite	**17**	3.2	89	8.70	83.8±6.6	97	0	87.2±9.3	12.4	1.4	31	1.1
RHF 4	**21HLK04**	93.903	42.968	1317	Granite	**23**	9.19	385	26.39	70.3±4.8	17	10	72.6±4.0	-		-	-

Note: Uranium content of all grains measured by LA-ICP-MS. Pooled AFT ages of all grains. Central age calculated using the RadialPlotter program (Vermeesch, 2009).

https://doi.org/10.5194/egusphere-2024-3668
Preprint. Discussion started: 17 December 2024

4.2 Apatite fission-track dating

4.2.1 Methods

Apatite grains were concentrated using standard heavy-liquid and magnetic separation techniques prior to being mounted in epoxy resin on glass slides. The mounted grains were subsequently ground and polished to expose their internal surfaces. These polished mounts were etched in 5*M* HNO_3 for 20 seconds at 20 °C, following the protocols established by Gleadow et al. (2002). Apatite grains with polished surfaces parallel to prismatic crystal faces and uniform track distributions were selected for analysis. High-resolution digital images were captured in both reflected and transmitted light at a total magnification of 1000x using a Zeiss Axio Imager M1m microscope and a 3.2 MP camera. Fission-track density, confined track lengths, and etch-pit diameters (D_{par}) were measured (analyst: Z. Zhao) utilizing the Trackwork and Fast track systems at the Hubei Key Laboratory of Critical Zone Evolution, School of Earth Sciences, China University of Geosciences, Wuhan. The uranium content of selected grains was analysed using Laser Ablation-Inductively Coupled Plasma-Mass Spectrometry (LA-ICP-MS). Trace-element signals were normalized against ^{43}Ca using NIST-610 as a reference standard (Pearce et al., 1997; Vermeesch, 2017). AFT ages were calibrated using the LA-ICP-MS ζ method, with Fish Canyon Tuff apatite (28.4 ± 0.1 Ma) serving as the ζ calibration standard (Hasebe et al., 2004, 2013; Vermeesch, 2017).

4.2.2 Results

AFT ages for 16 samples from the Harlik Mountains span from the Early Cretaceous to early Paleocene (110.6 ± 6.5 to 50.5 ± 3.8 Ma). Mean track lengths (MTL) were measured for 15 of these samples, ranging from ~12.9 to ~12.0 μm (**Table 1**). **Figure S3** presents the confined AFT length distributions for each sample. Most bedrock samples passed the chi-squared test (Galbraith and Laslett, 1993); radial plots for each sample are provided in **Figure S4**.

All but two samples (19HLK27 and 19HLK28) from the low-relief surfaces show late Early Cretaceous AFT ages (~110-100 Ma; **Table 1**; **Fig. 5**), consistent with previously published AFT and apatite (U-Th)/He dates from nearby locations (Zhu et al., 2006; Gillespie et al., 2017a; Zhang et al., 2023). The single-grain age dispersions in these samples are relatively low (see **Figure S4**), with MTLs ranging from ~12.8 μm (n=58) to ~12.0 (n=43), and D_{par} ranging from ~1.4 to ~1.0 μm (**Table 1**). In contrast, two samples (19HLK27 and 19HLK28) obtained from relict surface S8 yielded Late Cretaceous AFT ages of 70 ± 6 Ma and 84 ± 7 Ma, respectively. Sample 19HLK27 has a MTL of ~12.6 μm (n=50), while sample 19HLK28 has a MTL of ~12.4 μm (n=31).

Samples from the right-lateral strike-slip fault zones dissecting the relict surfaces primarily exhibit Late Cretaceous AFT ages (~90-70 Ma; **Table 1**; **Fig. 5**). A sample collected from fault RHF 1 (23HLK02) has an AFT age of 90 ± 5 Ma, with a MTL of ~12.9 μm (n=100). Samples adjacent to the RHF 2 fault zone (19HLK07/08/10-1) range in age from 73 to 84 Ma, with MTLs of ~12.1 μm (n=140), ~12.4 μm (n=82), and ~12.6 μm (n=61), respectively. One of these samples (19HLK07) did not pass the chi-squared test (**Table 1**; **Figure S4**). Three samples (19HLK17/22/24) located within the RHF 3 fault zone record AFT ages ranging from 74 to 80 Ma, with MTLs of ~12.1 μm (n=35), ~12.4 μm (n=28), and ~12.9 μm (n=18), respectively. A single sample (21HK04) was collected from RHF 4, yielding an AFT age of 70 ± 5 Ma.

https://doi.org/10.5194/egusphere-2024-3668
Preprint. Discussion started: 17 December 2024

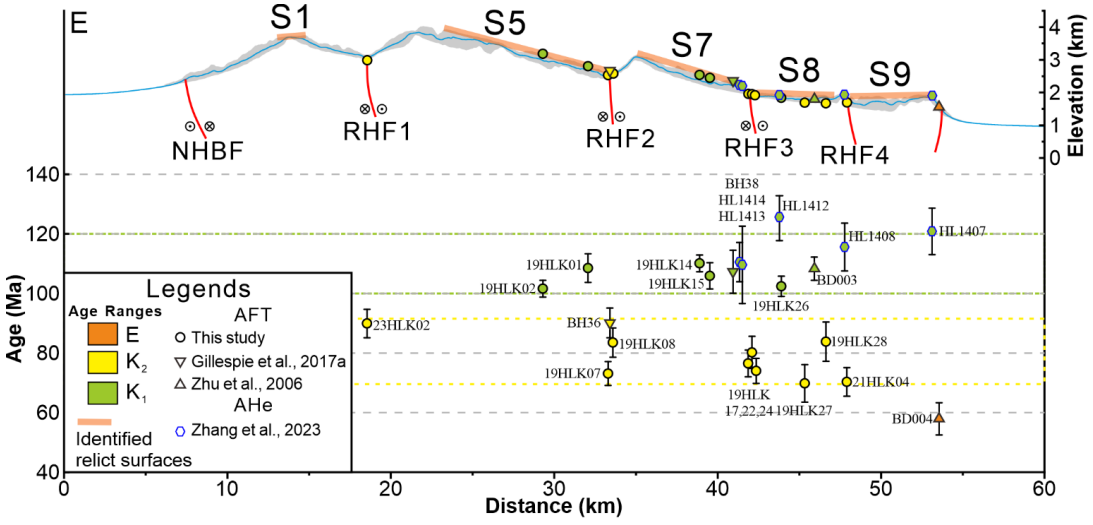

Figure 5: AFT and (U-Th)/He data projected onto profile E-E'. AFT and (U-Th)/He data from different sources are plotted with different symbols; colours indicate ages (green: Early Cretaceous; yellow: Late Cretaceous; orange: Paleogene).

4.3 Thermal History Modeling

4.3.1 Methods

To characterize the cooling history of rocks from various geomorphic units and tectonic locations, we employed inverse thermal-history modelling using QTQt software (version 5.8.0) to generate likely time-temperature (t-T) paths (Gallagher, 2012). QTQt utilizes a Bayesian Markov Chain Monte Carlo approach, allowing users to input thermochronometric data and define t-T constraints. The model output presents a population of acceptable thermal histories that define a posterior probability distribution. The "expected" path represents the weighted mean thermal history derived from this posterior distribution. For modelling purposes, the samples were divided into two categories: relict-surface samples (**Fig. 6**) and fault-zone samples (**Fig. 7**). Additionally, thermal histories were modelled for the two younger samples (19HLK27 and 19HLK28) collected from the low-relief surface S8 to explore potential causes for these anomalously young ages.

The AFT data were modelled using the multi-kinetic annealing model of Ketcham et al. (2007), with Dpar serving as the kinetic parameter. Inversion was constrained solely by the current surface temperature, which was set at 10 ± 10 °C. General prior ranges were established as AFT central age ± AFT central age for time and 70 ± 70℃ for temperature. The software executed 200,000 burn-in iterations followed by 200,000 post-burn-in iterations to achieve stable results. For discussion purposes, cooling rates are classified empirically into three categories: slow (< 0.5°C/Ma), moderate (0.5-2°C/Ma), and rapid (> 2°C/Ma) cooling (He et al., 2022a).

4.3.2 Results

The modeling results for sample 19HLK02 from surface S5 indicates a relatively steady cooling trajectory since ~130 Ma, with a phase of moderate cooling occurring between 130 and 100 Ma (~0.9 °C/Ma; **Fig. 6a**). Similarly, samples from surface S7 (19HLK14 and 19HLK15) exhibit steady cooling since ~130 Ma, with accelerated cooling rates during the 130-100 Ma interval (1.1 °C/Ma) compared to the post-100 Ma phase (0.5 °C/Ma; **Fig. 6b**).

In contrast, the thermal history of samples collected from surface S8 is more variable. Sample 19HLK26, situated away from the fault boundaries, displays a thermal history akin to that of the sample from surface S5, showing moderate cooling (0.8 °C/Ma) in the late Early Cretaceous, followed by slow cooling (< 0.5°C/Ma; **Fig. 6c**). Conversely, samples 19HLK27 and

https://doi.org/10.5194/egusphere-2024-3668
Preprint. Discussion started: 17 December 2024

19HLK28 record cooling starting at ~90 Ma, with a relatively rapid cooling rate of 1.9 °C/Ma until 70 Ma, which is faster than the cooling rate observed for sample 19HLK26 during the 130-100 Ma phase (**Fig. 6d**).

Overall, the QTQt modelling results for samples collected from the relict surfaces in the Harlik Mountains indicate a rapid cooling phase between 130 and 100 Ma, followed by a period of stable, slow cooling. Notably, some samples from surface S8 also experienced accelerated cooling 20-30 Ma later, around 90-70 Ma. All modelled thermal histories also suggest somewhat more rapid cooling from ~40 °C to surface temperatures during the last ~20 Ma.

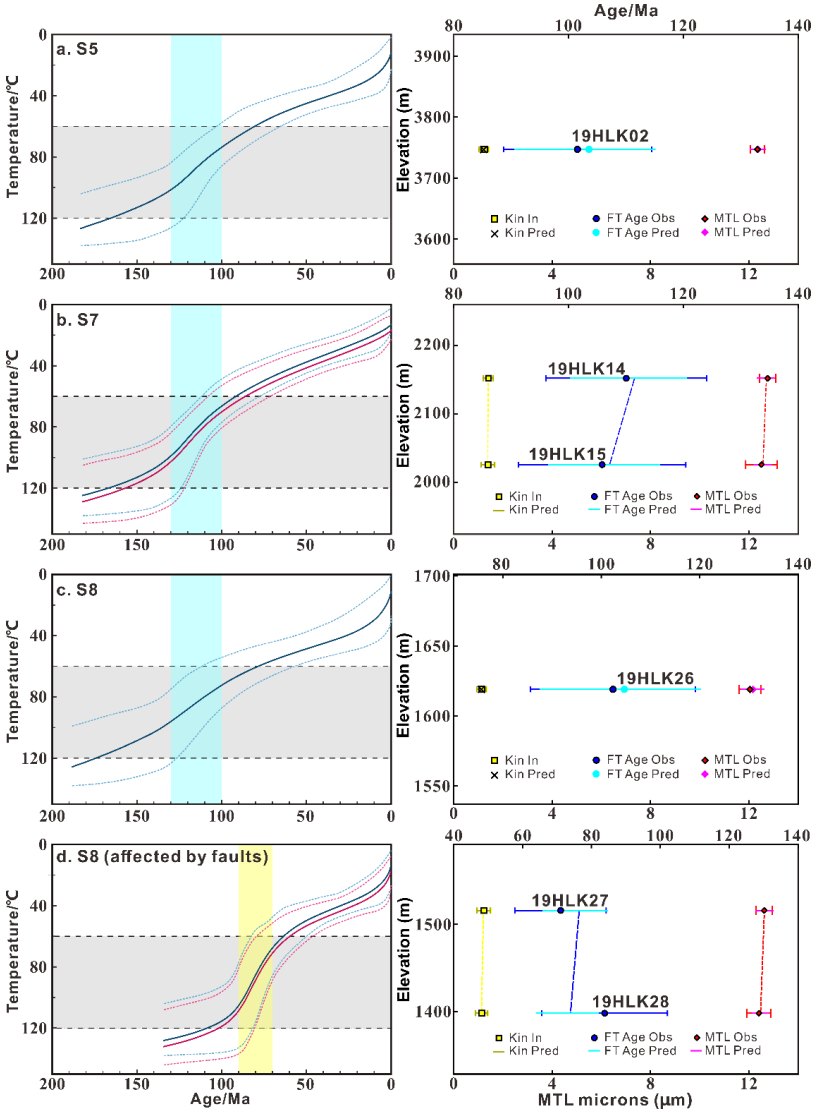

Figure 6: Thermal history models based on AFT data for samples from relict surfaces on the southern slopes of the Harlik Mountains (easternmost Tianshan) generated using QTQt software (Gallagher, 2012). Right panels show fit to the observed AFT ages and MTL.

Samples from the fault zones RHF 2 (19HLK07) and RHF 3 (19HLK17, 19HLK22, and 19HLK24) exhibit similar t-T paths, characterized by rapid cooling during the Late Cretaceous (~90-70 Ma) at a rate of ~1.8 °C/Ma (**Fig. 7b-c**), followed by a transition to slower cooling. The thermal history of RHF 1 (23HLK02) is comparable to that of samples from RHF 2 and RHF 3, but it records a slightly earlier rapid cooling phase (2.3 °C/Ma) around 100-90 Ma (**Fig. 7a**). These thermal histories also show rapid late-stage cooling from 40-50 °C to surface temperatures during the last 10-20 Ma.

https://doi.org/10.5194/egusphere-2024-3668
Preprint. Discussion started: 17 December 2024

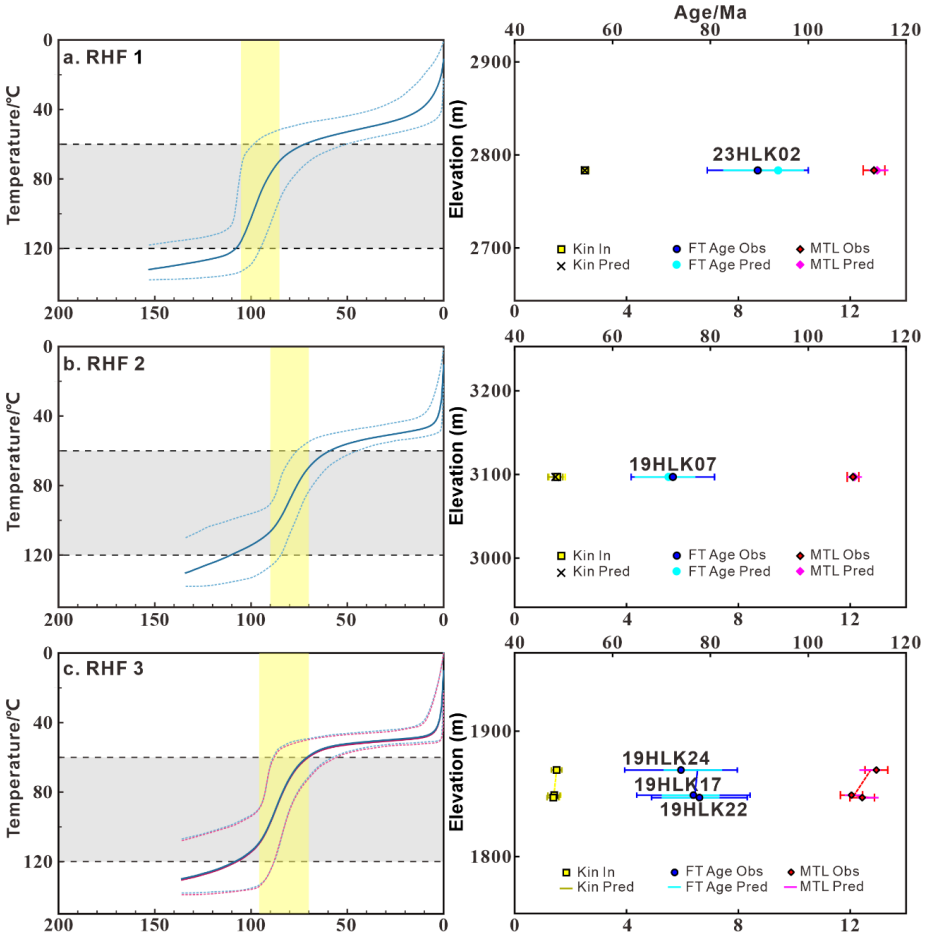

Figure 7: Thermal history models based on AFT data for samples from fault zones on the southern slopes of the Harlik Mountains (easternmost Tianshan) generated using QTQt software (Gallagher, 2012). Right panels show fit to the observed AFT ages and MTL.

5. Discussion

5.1 Early Cretaceous exhumation of the Eastern Tianshan

Thermal history models for samples from the low-relief surfaces record a relatively rapid exhumation and cooling event during the Early Cretaceous in the Eastern Tianshan (**Fig. 8**). Such a thermal history contrasts to that in the Yili block (Wang et al., 2018; He et al., 2022b), Chinese Central Tianshan (Jolivet et al., 2010), and the Jueluotage Range (Sun et al., 2021), where exhumation is less pronounced during the Late Jurassic to Early Cretaceous. The low-relief surfaces formed during the Jurassic in the Central Tianshan were maintained under these relatively stable conditions (Jolivet et al., 2010; He et al., 2021b, 2022b). Cooling during the Late Jurassic to Early Cretaceous was more significant in the Kyrgyz Tianshan compared to the Chinese Western Tianshan (Sobel et al., 2006a; De Grave et al., 2012; De Pelsmaeker et al., 2015). The spatial distribution of this exhumation event in the Kyrgyz Tianshan and the Chinese Western Tianshan (**Fig. 1**) suggests propagation of uplift and exhumation from the southwest towards the northeast, consistent with deformation and exhumation driven by the collision of the Lhasa block with Eurasia during the Late Jurassic to Early Cretaceous (~160-120 Ma; Kapp et al., 2007; Ma et al., 2017; Lai et al., 2019; Hu et al., 2022).

https://doi.org/10.5194/egusphere-2024-3668
Preprint. Discussion started: 17 December 2024

Importantly, the available thermochronological data from the low-relief surfaces in the Harlik Mountains do not indicate any cooling events predating the Cretaceous. Evidence of rapid cooling prior to the Early Cretaceous is also limited in the easternmost Tianshan, with a signal of Triassic cooling preserved only on the fringes of the region, outside the main fault-bound ranges (Gillespie et al., 2017a; Chen et al., 2020a). Sedimentological evidence indicates that the easternmost Tianshan was characterized by an extensional environment during the Late Triassic to Middle Jurassic, with relatively gentle topography (Chen et al., 2019). This implies that low-relief topography likely existed in the easternmost Tianshan prior to the Early Cretaceous, but was subsequently altered by tectonic deformation and associated exhumation during this period (**Fig. 8b**).

The compressional deformation identified in the Junggar basin, easternmost Tianshan, Turpan-Hami basin, and Beishan regions during the Middle to Late Jurassic (Zhu et al., 2004; Chen et al., 2020a; Guan et al., 2021; Liu et al., 2023) was likely influenced by the initial closure of the western Mongol-Okhotsk Ocean and Lhasa–Qiangtang collision (Zhang et al., 2019; Wang et al., 2022; Liu et al., 2023). However, low-temperature thermochronology records in regions such as the easternmost Tianshan, East Junggar, Beishan, Gobi-Altai, and Sayan-Altai predominantly record cooling during the middle Cretaceous (Jolivet et al., 2007; Glorie et al., 2012a; De Grave et al., 2014; Chen et al., 2020a, b; He et al., 2022a; Liu et al., 2023). Cooling associated with normal-fault footwall exhumation during the mid to late Early Cretaceous is recorded in the Barkol Mountains (128-110 Ma; Chen et al., 2020b) as well as in in the Beishan area (~124-115 Ma; Liu et al., 2023). Early Cretaceous rift-related basalts (~126–99 Ma) are also common in southern Mongolia, Alxa block, and northern Qilian Shan (Graham et al., 2001; Tang et al., 2012; Hui et al., 2021). The normal faults and basalts mentioned above are considered to be associated with late-Mesozoic regional crustal extension (Chen et al., 2003; Meng, 2003; Liu et al., 2023). By this time, significant deformation associated with the Lhasa collision or the closure of the Mongol-Okhotsk Ocean had ceased (Wang et al., 2015; Yang et al., 2015b; Li et al., 2017; Ma et al., 2017), making it unlikely that the cooling during this period in the easternmost Tianshan can be directly attributed to far-field effects related to these orogenies. It is plausible that subsequent tectonic events, such as the collapse of the Mongol-Okhotsk orogen (~145-100 Ma; Donskaya et al., 2008; Wang et al., 2015; Yang et al., 2015b) and break-off of the Bangong-Nujiang Ocean slab (latest Early Cretaceous; Sui et al., 2013; Wu et al., 2015; Liu et al., 2018), played significant roles in shaping the landscape of the study area. Given that the break-off of the Bangong-Nujiang Ocean slab occurred later and was relatively short-lived, the collapse of the Mongol-Okhotsk orogen is more likely to have provided an extensional setting for the easternmost Tianshan and adjacent areas during the mid-to-late Early Cretaceous.

On the other hand, climate change may have accelerated erosion in the Eastern Tianshan and Altai regions during the mid-Cretaceous (Hendrix et al., 1992; Pullen et al., 2020; Jepson et al., 2021a). Sedimentary records from the Junggar basin indicate a transition from arid to semi-arid conditions during the Jurassic-Early Cretaceous, evolving into seasonally wet conditions by the middle Cretaceous (Hendrix et al., 1992; Allen and Vincent, 1997; Eberth et al., 2001). Prior to ~135 Ma, the depositional environment of the Turpan-Hami Basin transitioned from an erg environment characterized by extensive eolian cross-bedded sandstones of the Liushuquan Formation to a fluvial-lacustrine setting represented by the Dahaidao Formation (Wang et al., 2017; Zheng et al., 2023; Zhang et al., 2024). The Liushuquan Formation is dominated by medium- to fine-grained sandstones exhibiting planar and trough cross-stratification, indicative of a wind-dominated erg system with widespread dune development (Zhang et al., 2024), whereas the Dahaidao Formation consists mainly of gray-white sandstones deposited in a lacustrine setting with evidence of nesting pterosaurs, indicating a shift towards more stable, water-dominated conditions (Wang et al., 2017; Zhang et al., 2024). Although positive topography may have developed in the easternmost Tianshan by the Middle to Late Jurassic, the arid climate may have limited significant erosion. Conversely, the humid climate of the mid-Cretaceous likely could have intensified erosion, contributing to fluvial-lacustrine sedimentation in the surrounding basins.

5.2 Local fault activity during the Late Cretaceous to early Paleogene

Our geomorphological and structural analysis reveals that several right-lateral strike-slip faults segment the relict surfaces on the southern flank of the Harlik Mountains (**Fig. 3**). AFT ages from samples collected within these fault zones are mainly Late

https://doi.org/10.5194/egusphere-2024-3668
Preprint. Discussion started: 17 December 2024

Cretaceous (~90-70 Ma), notably younger than the cooling ages (>100 Ma) recorded in the surrounding low-relief surfaces. Rock cooling generally results from erosional or tectonic (normal-faulting controlled) exhumation, or from thermal disturbance. However, our observations show no significant differential erosion between these fault zones and the surrounding regions. Given that the faults are classified as right-lateral strike-slip rather than normal faults, the most plausible explanation for the differing cooling ages is thermal disturbance within the fault zones. Microstructural analysis of the rocks within these zones provides clear evidence for the presence of siliceous and carbonate fluids, indicating that these rocks were influenced by hydrothermal activity associated with faulting (**Fig. 4j-l**). This hydrothermal activity may have reset the AFT system in these rocks (**Fig. 8d**). Consequently, the observed cooling ages establish a minimum timing for fault activity, suggesting that faulting occurred during the 90-70 Ma interval. Concurrently, the cooling rate of the rocks on the relict low-relief surfaces began to slow down, indicating that regional uplift and erosion were gradually diminishing (**Fig. 8c**). During this time, deformation in the Eastern Tianshan was primarily governed by these right-lateral strike-slip faults.

Throughout the Late Cretaceous, both the northern and southern tectonic belts of the Tianshan exhibited relatively low levels of tectonic activity. Consequently, many of the relict low-relief surfaces in the Tianshan region are believed to have formed during this period (Sobel et al., 2006b; Chen et al., 2018, 2020b). While records of cooling events during the Late Cretaceous are less frequent than those from the Early Cretaceous, such records are widely distributed across Central Asia (Sobel et al., 2006a; Jolivet et al., 2010; Glorie et al., 2012a, b; De Grave et al., 2013, 2014; De Pelsmaeker et al., 2015; Chen et al., 2020a). In the Tethys tectonic domain, the collision and amalgamation of island arcs like Kohistan, Dras, and Ladakh (**Fig. 8**; Yuan et al., 2021; Andjic et al., 2022) are thought to have generated a compressive stress field, reactivating inherited Paleozoic structures within the Western Tianshan (Schwab et al., 2004; Jolivet et al., 2010; Chen et al., 2018). During the Late Cretaceous and early Paleogene, with the exception of these localized fault zones, the broader Western Tianshan experienced slow cooling or tectonic quiescence, facilitating the development of widespread planation surfaces (e.g., Bazhenov, 1993; Burbank et al., 1999; Glorie et al., 2010).

The Mongol-Okhotsk orogeny and subsequent orogenic collapse occurred mainly in the Late Jurassic to Early Cretaceous, but its influence appears to have extended into the Late Cretaceous, characterized by fault reactivation in an extensional tectonic regime (van der Beek et al., 1996; Jolivet et al., 2009; Glorie et al., 2012a; De Grave et al., 2014). Evidence for Late Cretaceous cooling events within a northeast-southwest extensional context has been reported in the Eastern Tianshan (Song et al., 2023), Altai (Glorie et al., 2012b), Siberian Altai (Glorie et al., 2012a), Sayan (De Grave et al., 2014) and Beishan (Liu et al., 2023; Wang et al., 2024), bearing witness to a widespread Late Cretaceous fault reactivation event (**Fig. 1**). In the Harlik Mountains, the fault activity recorded between 90-70 Ma likely represents a similar fault reactivation event. Comparing the tectonic settings recorded in the northern (Glorie et al., 2012a; De Grave et al., 2014) and southern (Yuan et al., 2021; Andjic et al., 2022) tectonic belts of the Tianshan during this period suggests that Late-Cretaceous fault (re)activation in the easternmost Tianshan is likely associated with extensional tectonics resulting from the collapse of the Mongol-Okhotsk Orogen. The aridification of the climate since the Late Cretaceous would have limited the amount of exhumation during this period (Jepson et al., 2021a).

5.3 Cenozoic Reactivation of the Eastern Tianshan

During the period from 90 to 70 Ma, the active right-lateral strike-slip faults in the Eastern Tianshan did not induce significant differential exhumation, and rapid exhumation ceased across most areas since that time. Thermal modeling indicates a marked slowdown in cooling rate for low-relief surface samples after 100 Ma, likely coinciding with the onset of planation.

During the Cenozoic, activity in the Mongol-Okhotsk tectonic belt largely diminished. To the south of the Tianshan, the collision between the southwestern margin of the Eurasian and Indian continents led to multi-stage uplift and expansion of the Qinghai-Tibetan Plateau (**Fig. 8**; Wang et al., 2011; van Hinsbergen et al., 2012; Ding et al., 2022; Suo et al., 2022). The

https://doi.org/10.5194/egusphere-2024-3668
Preprint. Discussion started: 17 December 2024

Cenozoic India-Eurasia collision caused significant deformation in the Tianshan and surrounding regions, reactivating pre-existing structures from the Paleozoic amalgamation and subsequent intra-continental deformation (Molnar and Tapponnier, 1975; Burchfiel et al., 1999). Low-temperature thermochronology analyses indicate that the recent and ongoing deformation and reactivation in the Tianshan began in the Oligocene-Miocene (De Grave et al., 2007; Chen et al., 2022; Wang et al., 2023b; Jiang et al., 2024), marking the formation of the modern Tianshan topography. In the Eastern Tianshan, the left-lateral strike-slip Gobi-Tianshan Fault was reported to be active during the Cenozoic (Cunningham et al., 2003), although direct age constraints for its Cenozoic activity are lacking. This fault developed into a positive flower system in the Harlik Mountains, functioning as a restraining bend for the left-lateral strike-slip fault (Cunningham et al., 2003; Cunningham, 2007). This fault system facilitated the exhumation of the Harlik Mountains and the tilting of previously formed planation surfaces (Cunningham et al., 2003; Cunningham, 2007; Gillespie et al., 2017a). Consequently, the more rapid cooling identified after ~30 Ma in our thermal models likely corresponds to this late-stage exhumation phase. Moreover, following a period of non-deposition from the Late Cretaceous to the Eocene (Shen et al., 2020), the Turpan-Hami and Barkol basins began to receive sediments again during the Oligocene to Miocene (Chen et al., 2019; Ding et al., 2024). This renewed sedimentation indicates that the Harlik Mountains have been more actively eroding since that time, marking the conclusion of relict surface development and initiating a new phase of landscape evolution in the region (**Fig. 8e**).

Recent apatite (U-Th)/He (AHe) data from the erosion surfaces of the southern Harlik Mountains (Zhang et al., 2023) show similar late Early Cretaceous ages as our AFT data, supporting rapid cooling during this time interval. Morevoer, these data limit the amount of Cenozoic exhumation in the Harlik Mountains to less than 2 km, assuming a thermal gradient of 25 °C/km and a closure temperature of ~50 °C for AHe. Shen et al. (2024) have recently documented that the Gobi-Tian Shan Fault (GTF) is active in the Quaternary, with left-lateral slip rates of 1.1–1.4 mm/yr and approximately 0.7 mm/yr of north–south crustal shortening across the Harlik Mountains. However, few Oligocene AHe ages have been reported from the Barkol Mountains, potentially linked to tectonic activity, including fault reactivation (Zhang et al., 2023). Therefore, the vertical displacement on major faults in the easternmost Tianshan may be associated with only limited erosion, as also observed in the western Chinese Tian Shan (Charreau et al., 2017; 2023). The Cenozoic climate of the easternmost Tianshan, characterized by aridity as revealed by paleoclimate simulations (Jepson et al., 2021a), led to limited erosion, primarily confined to river valleys and the mountain front. Therefore, due to the weak Cenozoic tectonic uplift and limited surface erosion, crustal exhumation was insufficient to induce cooling of the basement and produce younger thermochronological ages. These conditions allowed the preservation of large-scale Mesozoic low-relief surfaces in the Harlik Mountains, even though they were deformed and tilted during late Cenozoic compression.

https://doi.org/10.5194/egusphere-2024-3668
Preprint. Discussion started: 17 December 2024

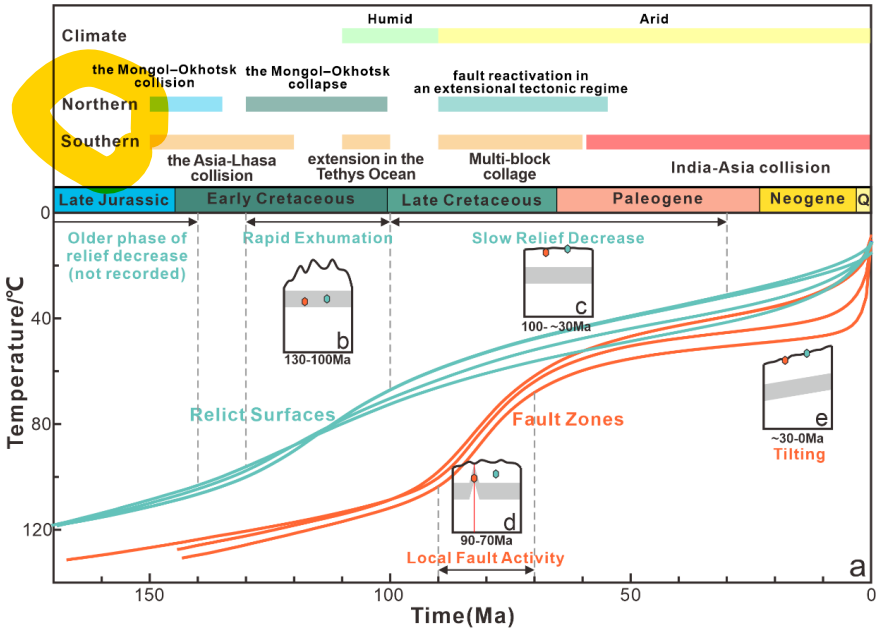

Figure 8: a. The geomorphological and tectonic significance of the inferred exhumation history of the Harlik Mountains (time-temperature curves for the relict surfaces in green and fault zones in red); possible driving factors are indicated in top panel; b-e. Sketch of the envisaged evolution of the relict surfaces and relative location of samples located on the relict surface (green) and in the fault zones (red): b. Rapid exhumation; c. Slow relief decrease; d. Local fault activity; e. Tilting.

6. Conclusions

This study integrates new thermochronological, structural, and geomorphological data to elucidate the Mesozoic-Cenozoic evolution of the Harlik Mountains in the easternmost Tianshan. Relict surfaces, identified and mapped through digital terrain analysis, reveal the impact of regional faulting and tectonic activity on landscape evolution. The following summarizes the main evolutionary phases:

1. **Early Cretaceous (130-100 Ma):** Rapid exhumation and cooling in the Harlik Mountains were driven by tectonic processes linked to the collapse of the Mongol-Okhotsk orogen. Mid-Cretaceous climate shifts promoted erosion, contributing to basin sedimentation and landscape modification.

   Late Cretaceous to Early Paleogene (90-70 Ma): Right-lateral strike-slip faulting under an extensional regime dissected the relict surfaces, although overall landscape changes were limited. Late-Cretaceous cooling and fault reactivation likely stemmed from the ongoing collapse of the Mongol-Okhotsk orogen, with a transition to an arid climate limiting further erosion. Formation of the low-relief surfaces started during this time, marked by a slowdown in cooling and exhumation rates.

2. **Late Cenozoic (~30 Ma to present):** Renewed tectonic activity associated with the far-field effects of the India-Eurasia collision uplifted and tilted the Harlik Mountains, marking the development of modern topography. Low erosion rates preserved Mesozoic low-relief surfaces despite continued fault activity and basin sedimentation.

In conclusion, the Mesozoic-Cenozoic evolution of the Eastern Tianshan landscape reflects a complex interplay of tectonic reactivation, faulting, and climatic influences, with thermochronological and structural evidence highlighting the preservation and transformation of low-relief surfaces in response to regional tectonics and environmental shifts.

https://doi.org/10.5194/egusphere-2024-3668
Preprint. Discussion started: 17 December 2024

Code availability. The QTQt software used for thermal-history modeling and inverse modeling of thermochronological data was developed by Kerry Gallagher and is publicly available at https://www.iearth.edu.au/codes/QTQt/ (Gallagher, 2012). The RadialPlotter program, used for calculating central ages of apatite fission-track data and generating radial plots, was developed by Pieter Vermeesch and is available for download at https://www.ucl.ac.uk/~ucfbpve/radialplotter/ (Vermeesch, 2009).

Data availability. The compilation of data is available in the Supplement.

Supplement. The supplement related to this article is available online.

Author contributions. ZZ: Conceptualization, data curation, formal analysis, investigation, methodology, visualization, fieldwork, sample collection, manuscript draft writing and revision; TS: Data curation, Investigation, Methodology, Validation, Project design, regional geology, fieldwork, sample collection, manuscript revision; GW: Project administration, funding acquisition, investigation, supervision, fieldwork, manuscript revision; PvdB: Data curation, manuscript revision; YZ: Data curation, investigation; CM: Data curation, investigation.

Competing interests. The authors declare that they have no conflict of interest.

Acknowledgements. We sincerely thank Chengyu Zhu (China University of Geosciences) and Jie Wei (China University of Geosciences) for fission-track dating support, as well as Wei Wang (China University of Geosciences) for field work assistance.

Financial support. This study was funded by the Key Program of the National Natural Science Foundation of China (grant No. 42430307), the National Natural Science Foundation of China (grants No. 42172251, and No. 41972208), and Geological Survey Projects of the China Geological Survey (grants DD20179607, and DD20160060). We gratefully acknowledge the financial support from the China Scholarship Council (CSC, No. 202306410183) for funding research of Z. Zhao stay in Germany.

Review statement.

https://doi.org/10.5194/egusphere-2024-3668
Preprint. Discussion started: 17 December 2024

References

Allen, M. B. and Vincent, S. J.: Fault reactivation in the Junggar region, northwest China: The role of basement structures during Mesozoic-Cenozoic compression, Journal of the Geological Society, 154, 151–155, https://doi.org/10.1144/gsjgs.154.1.0151, 1997.

Allen, M. B., Alsop, G. I., and Zhemchuzhnikov, V. G.: Dome and basin refolding and transpressive inversion along the Karatau Fault System, southern Kazakstan, Journal of the Geological Society, 158, 83–95, https://doi.org/10.1144/jgs.158.1.83, 2001.

Andjic, G., Zhou, R. J., Jonell, T. N., and Aitchison, J. C.: A Single Dras-Kohistan-Ladakh Arc Revealed by Volcaniclastic Records, Geochem. Geophys. Geosyst., 23, 22, https://doi.org/10.1029/2021gc010042, 2022.

Bande, A., Sobel, E. R., Mikolaichuk, A., and Torres Acosta, V.: Talas–Fergana Fault Cenozoic timing of deformation and its relation to Pamir indentation, Geological Society, London, Special Publications, 427, 295, https://doi.org/10.1144/SP427.1, 2015.

Bande, A., Sobel, E. R., Mikolaichuk, A., Schmidt, A., and Stockli, D. F.: Exhumation history of the western Kyrgyz Tien Shan: Implications for intramontane basin formation, Tectonics, 36, 163–180, https://doi.org/10.1002/2016tc004284, 2017.

Bazhenov, M. L.: Cretaceous paleomagnetism of the Fergana Basin and adjacent ranges, Central-Asia – tectonic implications, Tectonophysics, 221, 251–267, https://doi.org/10.1016/0040-1951(93)90335-h, 1993.

Bullen, M. E., Burbank, D. W., Garver, J. I., and Abdrakhmatov, K. Y.: Late Cenozoic tectonic evolution of the northwestern Tien Shan: New age estimates for the initiation of mountain building, Geological Society of America Bulletin, 113, 1544–1559, https://doi.org/10.1130/0016-7606(2001)113<1544:Lcteot>2.0.Co;2, 2001.

Burbank, D. W., McLean, J. K., Bullen, M., Abdrakhmatov, K. Y., and Miller, M. M.: Partitioning of intermontane basins by thrust-related folding, Tien Shan, Kyrgyzstan, Basin Res., 11, 75–92, https://doi.org/10.1046/j.1365-2117.1999.00086.x, 1999.

Burchfiel, B. C., Brown, E. T., Deng, Q. D., Feng, X. Y., Li, J., Molnar, P., Shi, J. B., Wu, Z. M., and You, H. C.: Crustal shortening on the margins of the Tien Shan, Xinjiang, China, International Geology Review, 41, 665–700, https://doi.org/10.1080/00206819909465164, 1999.

Calvet, M., Gunnell, Y., and Farines, B.: Flat-topped mountain ranges: Their global distribution and value for understanding the evolution of mountain topography, Geomorphology, 241, 255–291, https://doi.org/10.1016/j.geomorph.2015.04.015, 2015.

Cao, K., Tian, Y., van der Beek, P., Wang, G., Shen, T., Reiners, P., Bernet, M., and Husson, L.: Southwestward growth of plateau surfaces in eastern Tibet, Earth-Science Reviews, 232, 104160, https://doi.org/10.1016/j.earscirev.2022.104160, 2022.

Cao, L., Shao, L., Qiao, P., Zhao, Z., and van Hinsbergen, D. J. J.: Early Miocene birth of modern Pearl River recorded low-relief, high-elevation surface formation of SE Tibetan Plateau, Earth and Planetary Science Letters, 496, 120–131, https://doi.org/10.1016/j.epsl.2018.05.039, 2018.

Chang, J., Li, D., Min, K., Qiu, N. S., Xiao, Y., Wu, H., and Liu, N.: Cenozoic deformation of the Kalpin fold-and-thrust belt, southern Chinese Tian Shan: New insights from low-T thermochronology and sandbox 21odelling, Tectonophysics, 766, 416–432, https://doi.org/10.1016/j.tecto.2019.06.018, 2019.

Charreau, J., Saint-Carlier, D., Dominguez, S., Lavé, J., Blard, P.-H., Avouac, J.-P., Jolivet, M., Chen, Y., Wang, S., Brown, N. D., Malatesta, L. C., Rhodes, E., and Aster Team: Denudation outpaced by crustal thickening in the eastern Tianshan, Earth and Planetary Science Letters, 479, 179–191, https://doi.org/10.1016/j.epsl.2017.09.025, 2017.

https://doi.org/10.5194/egusphere-2024-3668
Preprint. Discussion started: 17 December 2024

Charreau, J., Blard, P.-H., Lavé, J., Dominguez, S., and Li, W. S.: Unsteady topography in the eastern Tianshan due to imbalance between denudation and crustal thickening, Tectonophysics, 848, 229702, https://doi.org/10.1016/j.tecto.2022.229702, 2023.

Charvet, J., Shu, L. S., Laurent-Charvet, S., Wang, B., Faure, M., Cluzel, D., Chen, Y., and de Jong, K.: Palaeozoic tectonic evolution of the Tianshan belt, NW China, Sci. China Earth Sci., 54, 166–184, https://doi.org/10.1007/s11430-010-4138-1, 2011.

Chen, H. L., Lin, X. B., Cheng, X. G., Gong, J. F., Bian, S., Wu, L., Jia, C. Z., Yang, S. F., Guo, Z. J., and Jia, D.: Two-phase intracontinental deformation mode in the context of India-Eurasia collision: insights from a structural analysis of the West Kunlun-Southern Junggar transect along the NW margin of the Tibetan Plateau, J. Geol. Soc., 179, 14, https://doi.org/10.1144/jgs2021-029, 2022.

Chen, X., Yin, A., Gehrels, G. E., Cowgill, E. S., Grove, M., Harrison, T. M., and Wang, X.: Two phases of mesozoic north-south extension in the eastern altyn tagh range, northern tibetan plateau, Tectonics, 22, 2001TC001336, https://doi.org/10.1029/2001TC001336, 2003.

Chen, Y., Wang, G. C., Zhao, X., Wang, Y. B., Ji, J. L., Cao, K., Shen, T. Y., Zhang, P., and Wang, A.: Evolution of the Barkol Basin, eastern Tian Shan, and its geodynamic background, International Journal of Earth Sciences, 108, 1253–1271, https://doi.org/10.1007/s00531-019-01704-y, 2019.

Chen, Y., Wang, G. C., Kapp, P., Shen, T. Y., Zhang, P., Zhu, C. Y., and Cao, K.: Episodic exhumation and related tectonic controlling during Mesozoic in the Eastern Tian Shan, Xinjiang, northwestern China, Tectonophysics, 796, https://doi.org/10.1016/j.tecto.2020.228647, 2020a.

Chen, Y., Wang, G. C., Shen, T. Y., Zhang, P., Sotiriou, P., and Zhu, C. Y.: Tectono-geomorphic evolution of Harlik Mountain in the Eastern Tian Shan, insight from thermochronological data and geomorphic analysis, Geol J, 55, 7322–7334, https://doi.org/10.1002/gj.3951, 2020b.

Chen, Z. L., Wang, Z. X., Han, F. B., Zhang, W. G., Zhang, Q., Zhou, Z. J., Wang, X. H., Xiao, W. F., Han, S. Q., Yu, X. Q., Sun, Y., Nurgazy, T., Latyshev, N., and Zailabidin, H.: Late Cretaceous-Cenozoic uplift, deformation, and erosion of the SW Tianshan Mountains in Kyrgyzstan and Western China, Int. Geol. Rev., 60, 1019–1037, https://doi.org/10.1080/00206814.2017.1365018, 2018.

China Geological Survey: Geological map of Chinese Tianshan and adjacent areas, scale 1:1,000,000, Xi'an Institute of Geology and Mineral Resource, Xi'an, China, 2007.

Choulet, F., Faure, M., Cluzel, D., Chen, Y., Lin, W., and Wang, B.: From oblique accretion to transpression in the evolution of the Altaid collage: New insights from West Junggar, northwestern China, Gondwana Research, 21, 530–547, https://doi.org/10.1016/j.gr.2011.07.015, 2012.

Choulet, F., Chen, Y., Cogne, J. P., Rabillard, A., Wang, B., Lin, W., Faure, M., and Cluzel, D.: First Triassic palaeomagnetic constraints from Junggar (NW China) and their implications for the Mesozoic tectonics in Central Asia, Journal of Asian Earth Sciences, 78, 371–394, https://doi.org/10.1016/j.jseaes.2013.01.023, 2013.

Clark, M. K., Royden, L. H., Whipple, K. X., Burchfiel, B. C., Zhang, X., and Tang, W.: Use of a regional, relict landscape to measure vertical deformation of the eastern Tibetan Plateau, J. Geophys. Res. F Earth Surf., 111, https://doi.org/10.1029/2005JF000294, 2006.

Cunningham, D.: Structural and topographic characteristics of restraining bend mountain ranges of the Altai, Gobi Altai and easternmost Tien Shan, Geological Society, London, Special Publications, 290, 219, https://doi.org/10.1144/SP290.7, 2007.

Cunningham, D.: Mountain building processes in intracontinental oblique deformation belts: Lessons from the Gobi Corridor, Central Asia, J Struct Geol, 46, 255–282, https://doi.org/10.1016/j.jsg.2012.08.010, 2013.

https://doi.org/10.5194/egusphere-2024-3668
Preprint. Discussion started: 17 December 2024

Cunningham, D. and Zhang, J.: China | Mongolia: Mesozoic-Cenozoic, Encyclopedia of Geology, 509–525, https://doi.org/10.1016/b978-0-08-102908-4.00164-8, 2021.

Cunningham, D., Owen, L. A., Snee, L. W., and Li, J. L.: Structural framework of a major intracontinental orogenic termination zone: the easternmost Tien Shan, China, Journal of the Geological Society, 160, 575–590, https://doi.org/10.1144/0016-764902-122, 2003.

De Grave, J. and Van den haute, P.: Denudation and cooling of the Lake Teletskoye Region in the Altai Mountains (South Siberia) as revealed by apatite fission-track thermochronology, Tectonophysics, 349, 145–159, https://doi.org/10.1016/s0040-1951(02)00051-3, 2002.

De Grave, J., Buslov, M. M., and Van den Haute, P.: Distant effects of India-Eurasia convergence and Mesozoic intracontinental deformation in Central Asia: Constraints from apatite fission-track thermochronology, Journal of Asian Earth Sciences, 29, 188–204, https://doi.org/10.1016/j.jseaes.2006.03.001, 2007.

De Grave, J., Van den haute, P., Buslov, M. M., Dehandschutter, B., and Glorie, S.: Apatite fission-track thermochronology applied to the Chulyshman Plateau, Siberian Altai Region, Radiation Measurements, 43, 38–42, https://doi.org/10.1016/j.radmeas.2007.11.068, 2008.

De Grave, J., Glorie, S., Buslov, M. M., Izmer, A., Fournier-Carrie, A., Batalev, V. Y., Vanhaecke, F., Elburg, M., and Van den haute, P.: The thermo-tectonic history of the Song-Kul plateau, Kyrgyz Tien Shan: Constraints by apatite and titanite thermochronometry and zircon U/Pb dating, Gondwana Res., 20, 745–763, https://doi.org/10.1016/j.gr.2011.03.011, 2011.

De Grave, J., Glorie, S., Ryabinin, A., Zhimulev, F., Buslov, M. M., Izmer, A., Elburg, M., Vanhaecke, F., and Van den Haute, P.: Late Palaeozoic and Meso-Cenozoic tectonic evolution of the southern Kyrgyz Tien Shan: Constraints from multi-method thermochronology in the Trans-Alai, Turkestan-Alai segment and the southeastern Ferghana Basin, Journal of Asian Earth Sciences, 44, 149–168, https://doi.org/10.1016/j.jseaes.2011.04.019, 2012.

De Grave, J., Glorie, S., Buslov, M. M., Stockli, D. F., McWilliams, M. O., Batalev, V. Y., and Van den Haute, P.: Thermo-tectonic history of the Issyk-Kul basement (Kyrgyz Northern Tien Shan, Central Asia), Gondwana Research, 23, 998–1020, https://doi.org/10.1016/j.gr.2012.06.014, 2013.

De Grave, J., De Pelsmaeker, E., Zhimulev, F. I., Glorie, S., Buslov, M. M., and Van den haute, P.: Meso-Cenozoic building of the northern Central Asian Orogenic Belt: Thermotectonic history of the Tuva region, Tectonophysics, 621, 44–59, https://doi.org/10.1016/j.tecto.2014.01.039, 2014.

De Pelsmaeker, E., Glorie, S., Buslov, M. M., Zhimulev, F. I., Poujol, M., Korobkin, V. V., Vanhaecke, F., Vetrov, E. V., and De Grave, J.: Late-Paleozoic emplacement and Meso-Cenozoic reactivation of the southern Kazakhstan granitoid basement, Tectonophysics, 662, 416–433, https://doi.org/10.1016/j.tecto.2015.06.014, 2015.

De Pelsmaeker, E., Jolivet, M., Laborde, A., Poujol, M., Robin, C., Zhimulev, F. I., Nachtergaele, S., Glorie, S., De Clercq, S., Batalev, V. Y., and De Grave, J.: Source-to-sink dynamics in the Kyrgyz Tien Shan from the Jurassic to the Paleogene: Insights from sedimentological and detrital zircon U-Pb analyses, Gondwana Research, 54, 180–204, https://doi.org/10.1016/j.gr.2017.09.004, 2018.

Deng, X.-H., Wang, J.-B., Pirajno, F., Wang, Y.-W., Li, Y.-C., Li, C., Zhou, L.-M., and Chen, Y.-J.: Re–Os dating of chalcopyrite from selected mineral deposits in the Kalatag district in the eastern Tianshan Orogen, China, Ore Geology Reviews, 77, 72–81, https://doi.org/10.1016/j.oregeorev.2016.01.014, 2016.

Ding, L., Kapp, P., Cai, F., Garzione, C. N., Xiong, Z., Wang, H., and Wang, C.: Timing and mechanisms of Tibetan Plateau uplift, Nat Rev Earth Environ, 3, 652–667, https://doi.org/10.1038/s43017-022-00318-4, 2022.

Ding, Y., Shen, T., Wang, G., and Ji, J.: Sedimentary and heavy mineral records for the oligocene–miocene exhumation of the easternmost tianshan, J. Earth Sci., 35, 449–461, https://doi.org/10.1007/s12583-022-1757-3, 2024.

https://doi.org/10.5194/egusphere-2024-3668
Preprint. Discussion started: 17 December 2024

Donskaya, T. V., Windley, B. F., Mazukabzov, A. M., Kroener, A., Sklyarov, E. V., Gladkochub, D. P., Ponomarchuk, V. A., Badarch, G., Reichow, M. K., and Hegner, E.: Age and evolution of late Mesozoic metamorphic core complexes in southern Siberia and northern Mongolia, J. Geol. Soc., 165, 405–421, https://doi.org/10.1144/0016-76492006-162, 2008.

Dumitru, T. A., Da, Z., Chang, E. Z., Graham, S. A., and Carroll, A. R.: Uplift, exhumation, and deformation in the Chinese Tian Shan, Memoir of the Geological Society of America, 194, 71–99, 2001.

Eberth, D. A., Brinkman, D. B., Chen, P.-J., Yuan, F.-T., Wu, S.-Z., Li, G., and Cheng, X.-S.: Sequence stratigraphy, paleoclimate patterns, and vertebrate fossil preservation in Jurassic-Cretaceous strata of the Junggar Basin, Xinjiang Autonomous Region, People's Republic of China, Canadian Journal of Earth Sciences, 38, 1627–1644, https://doi.org/10.1139/e01-067, 2001.

Galbraith, R. F. and Laslett, G. M.: Statistical models for mixed fission track ages, Nuclear Tracks and Radiation Measurements, 21, 459–470, https://doi.org/10.1016/1359-0189(93)90185-C, 1993.

Gallagher, K.: Transdimensional inverse thermal history modeling for quantitative thermochronology, J. Geophys. Res.-Solid Earth, 117, 16, https://doi.org/10.1029/2011jb008825, 2012.

Gao, H. L., Liu, G. X., He, J. G., Tian, M. M., and Che, Y. F.: Mesozoic Cenozoic uplift exhumation history of East Tianshan: Evidence from apatite fission track, Earth Science Frontiers, 21, 249-260 (in Chinese with English abstract), 2014.

Gilder, S., Chen, Y., Cogné, J.-P., Tan, X., Courtillot, V., Sun, D., and Li, Y.: Paleomagnetism of Upper Jurassic to Lower Cretaceous volcanic and sedimentary rocks from the western Tarim Basin and implications for inclination shallowing and absolute dating of the M-0 (ISEA?) chron, Earth and Planetary Science Letters, 206, 587–600, https://doi.org/10.1016/S0012-821X(02)01074-9, 2003.

Gilder, S. A., Gomez, J., Chen, Y., and Cogné, J.: A new paleogeographic configuration of the Eurasian landmass resolves a paleomagnetic paradox of the Tarim Basin (China), Tectonics, 27, 2007TC002155, https://doi.org/10.1029/2007TC002155, 2008.

Gillespie, J., Glorie, S., Jepson, G., Zhang, Z. Y., Xiao, W. J., Danisik, M., and Collins, A. S.: Differential Exhumation and Crustal Tilting in the Easternmost Tianshan (Xinjiang, China), Revealed by Low-Temperature Thermochronology, Tectonics, 36, 2142–2158, https://doi.org/10.1002/2017tc004574, 2017a.

Gillespie, J., Glorie, S., Xiao, W. J., Zhang, Z. Y., Collins, A. S., Evans, N., McInnes, B., and De Grave, J.: Mesozoic reactivation of the Beishan, southern Central Asian Orogenic Belt: Insights from low-temperature thermochronology, Gondwana Res, 43, 107–122, https://doi.org/10.1016/j.gr.2015.10.004, 2017b.

Gillespie, J., Glorie, S., Jepson, G., Zhimulev, F., Gurevich, D., Danisik, M., and Collins, A. S.: Inherited structure as a control on late Paleozoic and Mesozoic exhumation of the Tarbagatai Mountains, southeastern Kazakhstan, J Geol Soc London, https://doi.org/10.1144/jgs2020-121, 2021.

Gleadow, A. J. W., Belton, D. X., Kohn, B. P., and Brown, R. W.: Fission Track Dating of Phosphate Minerals and the Thermochronology of Apatite, Reviews in Mineralogy and Geochemistry, 48, 579–630, https://doi.org/10.2138/rmg.2002.48.16, 2002.

Glorie, S. and De Grave, J.: Exhuming the Meso-Cenozoic Kyrgyz Tianshan and Siberian Altai-Sayan: A review based on low-temperature thermochronology, Geoscience Frontiers, 7, 155–170, https://doi.org/10.1016/j.gsf.2015.04.003, 2016.

Glorie, S., De Grave, J., Buslov, M. M., Elburg, M. A., Stockli, D. F., Gerdes, A., and Van den Haute, P.: Multi-method chronometric constraints on the evolution of the Northern Kyrgyz Tien Shan granitoids (Central Asian Orogenic Belt): From emplacement to exhumation, Journal of Asian Earth Sciences, 38, 131–146, https://doi.org/10.1016/j.jseaes.2009.12.009, 2010.

Glorie, S., De Grave, J., Buslov, M. M., Zhimulev, F. I., Stockli, D. F., Batalev, V. Y., Izmer, A., Van den Haute, P., Vanhaecke, F., and Elburg, M. A.: Tectonic history of the Kyrgyz South Tien Shan (Atbashi-Inylchek) suture zone: The role of inherited structures during deformation-propagation, Tectonics, 30, https://doi.org/10.1029/2011tc002949, 2011.

https://doi.org/10.5194/egusphere-2024-3668
Preprint. Discussion started: 17 December 2024

Glorie, S., De Grave, J., Buslov, M. M., Zhimulev, F. I., Elburg, M. A., and Van den Haute, P.: Structural control on Meso-Cenozoic tectonic reactivation and denudation in the Siberian Altai: Insights from multi-method thermochronometry, Tectonophysics, 544, 75–92, https://doi.org/10.1016/j.tecto.2012.03.035, 2012a.

Glorie, S., De Grave, J., Delvaux, D., Buslov, M. M., Zhimulev, F. I., Vanhaecke, F., Elburg, M. A., and Van den Haute, P.: Tectonic history of the Irtysh shear zone (NE Kazakhstan): New constraints from zircon U/Pb dating, apatite fission track dating and palaeostress analysis, J Asian Earth Sci, 45, 138–149, https://doi.org/10.1016/j.jseaes.2011.09.024, 2012b.

Glorie, S., Otasevic, A., Gillespie, J., Jepson, G., Danisik, M., Zhimulev, F. I., Gurevich, D., Zhang, Z., Song, D., and Xiao, W.: Thermo-tectonic history of the Junggar Alatau within the Central Asian Orogenic Belt (SE Kazakhstan, NW China): Insights from integrated apatite U/Pb, fission track and (U-Th)/He thermochronology, Geoscience Frontiers, 10, 2153–2166, https://doi.org/10.1016/j.gsf.2019.05.005, 2019.

Glorie, S., Nixon, A. L., Jepson, G., Gillespie, J., Warren, C., Meeuws, F., Simpson, A., and Xiao, W.: Meso-Cenozoic Tectonic History of the Altai: New Insights From Apatite U-Pb and Fission Track Thermochronology for the Fuyun Area (Xinjiang, China), Tectonics, 42, e2022TC007692, https://doi.org/10.1029/2022TC007692, 2023.

Gong, L., Kohn, B. P., Zhang, Z. Y., Xiao, B., Wu, L., and Chen, H. Y.: Exhumation and Preservation of Paleozoic Porphyry Cu Deposits: Insights from the Yandong Deposit, Southern Central Asian Orogenic Belt, Econ Geol, 116, 607–627, https://doi.org/10.5382/econgeo.4812, 2021.

Graham, S. A., Hendrix, M. S., Johnson, C. L., Badamgarav, D., Badarch, G., Amory, J., Porter, M., Barsbold, R., Webb, L. E., and Hacker, B. R.: Sedimentary record and tectonic implications of Mesozoic rifting in southeast Mongolia, Geol Soc Am Bull, 113, 1560–1579, https://doi.org/10.1130/0016-7606(2001)113<1560:Sratio>2.0.Co;2, 2001.

Guan, X. T., Wu, C. D., Zhou, T. Q., Tang, X. Y., Ma, J., and Fang, Y. N.: Jurassic-Lower Cretaceous sequence stratigraphy and allogenic controls in proximal terrestrial environments (Southern Junggar Basin, NW China), Geol. J., 25, https://doi.org/10.1002/gj.4132, 2021.

Haider, V. L., Kropacek, J., Dunkl, I., Wagner, B., and von Eynatten, H.: Identification of peneplains by multi-parameter assessment of digital elevation models, Earth Surf Proc Land, 40, 1477–1492, https://doi.org/10.1002/esp.3729, 2015.

Hasebe, N., Barbarand, J., Jarvis, K., Carter, A., and Hurford, A. J.: Apatite fission-track chronometry using laser ablation ICP-MS, Chem. Geol., 207, 135–145, https://doi.org/10.1016/j.chemgeo.2004.01.007, 2004.

Hasebe, N., Tamura, A., and Arai, S.: Zeta equivalent fission-track dating using LA-ICP-MS and examples with simultaneous U–Pb dating, Island Arc, 22, 280–291, https://doi.org/10.1111/iar.12040, 2013.

He, Z., Wang, B., Ni, X., De Grave, J., Scaillet, S., Chen, Y., Liu, J., and Zhu, X.: Structural and kinematic evolution of strike-slip shear zones around and in the central Tianshan: Insights for eastward tectonic wedging in the southwest Central Asian orogenic belt, Journal of Structural Geology, 144, 104279, https://doi.org/10.1016/j.jsg.2021.104279, 2021a.

He, Z., Wang, B., Glorie, S., Su, W., Ni, X., Jepson, G., Liu, J., Zhong, L., Gillespie, J., and De Grave, J.: Mesozoic building of the Eastern Tianshan and East Junggar (NW China) revealed by low-temperature thermochronology, Gondwana Research, 103, 37–53, https://doi.org/10.1016/j.gr.2021.11.013, 2022a.

He, Z., Glorie, S., Wang, F., Zhu, W., Fonseca, A., Su, W., Zhong, L., Zhu, X., and De Grave, J.: A re-evaluation of the Meso-Cenozoic thermo-tectonic evolution of Bogda Shan (Tian Shan, NW China) based on new basement and detrital apatite fission track thermochronology, International Geology Review, 65, 2093–2112, https://doi.org/10.1080/00206814.2022.2121946, 2023.

He, Z., Song, S., Wang, F., Zhu, W., Shen, X., Glorie, S., Liang, Y., Zhong, L., and De Grave, J.: Late Mesozoic intra-continental reactivation of the southern Altai, Central Asia, GSA Bulletin, https://doi.org/10.13140/RG.2.2.27504.26884, 2024 (in press).

https://doi.org/10.5194/egusphere-2024-3668
Preprint. Discussion started: 17 December 2024

He, Z. Y., Wang, B., Nachtergaele, S., Glorie, S., Ni, X., Su, W., Cai, D., Liu, J., and De Grave, J.: Long-term topographic evolution of the Central Tianshan (NW China) constrained by low-temperature thermochronology, Tectonophysics, 817, 229066, https://doi.org/10.1016/j.tecto.2021.229066, 2021b.

He, Z. Y., Wang, B., Su, W. B., Glorie, S., Ni, X. H., Liu, J. S., Cai, D. X., Zhong, L. L., and De Grave, J.: Meso-Cenozoic thermo-tectonic evolution of the Yili block within the Central Asian Orogenic Belt (NW China): Insights from apatite fission track thermochronology, Tectonophysics, 823, 17, https://doi.org/10.1016/j.tecto.2021.229194, 2022b.

Hendrix, M. S., Graham, S. A., Carroll, A. R., Sobel, E. R., McKnight, C. L., Schulein, B. J., and Wang, Z. X.: Sedimentary record and climatic implications of recurrent deformation in the tian-shan - evidence from mesozoic strata of the north tarim, south junggar, and turpan basins, northwest China, Geological Society of America Bulletin, 104, 53–79, https://doi.org/10.1130/0016-7606(1992)104<0053:Sracio>2.3.Co;2, 1992.

Hetzel, R., Dunkl, I., Haider, V., Strobl, M., von Eynatten, H., Ding, L., and Frei, D.: Peneplain formation in southern Tibet predates the India-Asia collision and plateau uplift, Geology, 39, 983–986, https://doi.org/10.1130/g32069.1, 2011.

Hui, J., Cheng, H., Zhang, J., Zhang, K., Qu, J., and Zhang, B.: Early cretaceous continent basalts in the alxa block, NW China: Geochronology, geochemistry, and tectonic implications, International Geology Review, 63, 882–899, https://doi.org/10.1080/00206814.2020.1734974, 2021.

Jaiswara, N. K., Pandey, P., and Pandey, A. K.: Mio-Pliocene piracy, relict landscape and drainage reorganization in the Namcha Barwa syntaxis zone of eastern Himalaya, Sci Rep, 9, 17585, https://doi.org/10.1038/s41598-019-54052-x, 2019.

Jepson, G., Glorie, S., Konopelko, D., Gillespie, J., Danisik, M., Mirkamalov, R., Mamadjanov, Y., and Collins, A. S.: Low-Temperature Thermochronology of the Chatkal-Kurama Terrane (Uzbekistan-Tajikistan): Insights Into the Meso-Cenozoic Thermal History of the Western Tian Shan, Tectonics, 37, 3954–3969, https://doi.org/10.1029/2017tc004878, 2018a.

Jepson, G., Glorie, S., Konopelko, D., Mirkamalov, R., Danisik, M., and Collins, A. S.: The low-temperature thermo-tectonic evolution of the western Tian Shan, Uzbekistan, Gondwana Res, 64, 122–136, https://doi.org/10.1016/j.gr.2018.08.003, 2018b.

Jepson, G., Glorie, S., Konopelko, D., Gillespie, J., Danisik, M., Evans, N. J., Mamadjanov, Y., and Collins, A. S.: Thermochronological insights into the structural contact between the Tian Shan and Pamirs, Tajikistan, Terra Nova, 30, 95–104, https://doi.org/10.1111/ter.12313, 2018c.

Jepson, G., Carrapa, B., Gillespie, J., Feng, R., DeCelles, P. G., Kapp, P., Tabor, C. R., and Zhu, J.: Climate as the Great Equalizer of Continental-Scale Erosion, Geophysical Research Letters, 48, e2021GL095008, https://doi.org/10.1029/2021GL095008, 2021a.

Jepson, G., Glorie, S., Khudoley, A. K., Malyshev, S. V., Gillespie, J., Glasmacher, U. A., Carrapa, B., Soloviev, A. V., and Collins, A. S.: The Mesozoic exhumation history of the Karatau-Talas range, western Tian Shan, Kazakhstan-Kyrgyzstan, Tectonophysics, 814, 228977, https://doi.org/10.1016/j.tecto.2021.228977, 2021b.

Ji, H. J., Tao, H. F., Wang, Q., Ma, D. X., and Hao, L. W.: Petrography, geochemistry, and geochronology of Lower Jurassic sedimentary rocks from the Northern Tianshan (West Bogda area), Northwest China: Implications for provenance and tectonic evolution, Geol. J., 54, 1688–1714, https://doi.org/10.1002/gj.3263, 2019.

Jia, Y. Y., Fu, B. H., Jolivet, M., and Zheng, S.: Cenozoic tectono-geomorphological growth of the SW Chinese Tian Shan: Insight from AFT and detrital zircon U-Pb data, Journal of Asian Earth Sciences, 111, 395–413, https://doi.org/10.1016/j.jseaes.2015.06.023, 2015.

Jiang, Y., Lu, H., Yang, R., Pang, L., Jiao, R., Wang, Y., Pang, J., and Li, Y.: Two-stage exhumation, uplift, and basinward propagation of the tian shan during the late cenozoic, Earth-Science Reviews, 256, 104868, https://doi.org/10.1016/j.earscirev.2024.104868, 2024.

https://doi.org/10.5194/egusphere-2024-3668
Preprint. Discussion started: 17 December 2024

Jolivet, M.: Mesozoic tectonic and topographic evolution of Central Asia and Tibet: a preliminary synthesis, Geological Society, London, Special Publications, 427, 19–55, https://doi.org/10.1144/SP427.2, 2017.

Jolivet, M., Ritz, J. F., Vassallo, R., Larroque, C., Braucher, R., Todbileg, M., Chauvet, A., Sue, C., Arnaud, N., De Vicente, R., Arzhanikova, A., and Arzhanikov, S.: Mongolian summits: An uplifted, flat, old but still preserved erosion surface, Geology, 35, 871–874, https://doi.org/10.1130/g23758a.1, 2007.

Jolivet, M., De Boisgrollier, T., Petit, C., Fournier, M., Sankov, V. A., Ringenbach, J. C., Byzov, L., Miroshnichenko, A. I., Kovalenko, S. N., and Anisimova, S. V.: How old is the Baikal Rift Zone? Insight from apatite fission track thermochronology, Tectonics, 28, 21, https://doi.org/10.1029/2008tc002404, 2009.

Jolivet, M., Dominguez, S., Charreau, J., Chen, Y., Li, Y. G., and Wang, Q. C.: Mesozoic and Cenozoic tectonic history of the central Chinese Tian Shan: Reactivated tectonic structures and active deformation, Tectonics, 29, https://doi.org/10.1029/2010tc002712, 2010.

Jolivet, M., Barrier, L., Dauteuil, O., Laborde, A., Li, Q., Reichenbacher, B., Popescu, S. M., Sha, J. G., and Guo, Z. J.: Late Cretaceous-Palaeogene topography of the Chinese Tian Shan: New insights from geomorphology and sedimentology, Earth and Planetary Science Letters, 499, 95–106, https://doi.org/10.1016/j.epsl.2018.07.004, 2018.

Kapp, P., DeCelles, P. G., Gehrels, G. E., Heizier, M., and Ding, L.: Geological records of the Lhasa-Qiangtang and Indo-Asian collisions in the Nima area of central Tibet, Geol Soc Am Bull, 119, 917–932, https://doi.org/10.1130/B26033.1, 2007.

Kassner, A., Ratschbacher, L., Jonckheere, R., Enkelmann, E., Khan, J., Sonntag, B. L., Gloaguen, R., Gadoev, M., and Oimahmadov, I.: Cenozoic intracontinental deformation and exhumation at the northwestern tip of the India-Asia collisionsouthwestern Tian Shan, Tajikistan, and Kyrgyzstan, Tectonics, 35, 2171–2194, https://doi.org/10.1002/2015tc003897, 2016.

Ketcham, R. A., Carter, A., Donelick, R. A., Barbarand, J., and Hurford, A. J.: Improved modeling of fission-track annealing in apatite, American Mineralogist, 92, 799–810, https://doi.org/10.2138/am.2007.2281, 2007.

Lai, W., Hu, X. M., Garzanti, E., Xu, Y. W., Ma, A. L., and Li, W.: Early Cretaceous sedimentary evolution of the northern Lhasa terrane and the timing of initial Lhasa-Qiangtang collision, Gondwana Res., 73, 136–152, https://doi.org/10.1016/j.gr.2019.03.016, 2019.

Li, S., Guilmette, C., Ding, L., Xu, Q., Fu, J. J., and Yue, Y. H.: Provenance of Mesozoic clastic rocks within the Bangong-Nujiang suture zone, central Tibet: Implications for the age of the initial Lhasa-Qiangtang collision, J. Asian Earth Sci., 147, 469–484, https://doi.org/10.1016/j.jseaes.2017.08.019, 2017.

Liu, D.-L., Shi, R.-D., Ding, L., and Zou, H.-B.: Late Cretaceous transition from subduction to collision along the Bangong-Nujiang Tethys: New volcanic constraints from central Tibet, Lithos, 296–299, 452–470, https://doi.org/10.1016/j.lithos.2017.11.012, 2018.

Liu, F. L., Gao, H. S., Pan, B. T., Li, Z. M., and Su, H.: Quantitative analysis of planation surfaces of the upper Yangtze River in the Sichuan-Yunnan Region, Southwest China, Front Earth Sci-Prc, 13, 55–74, https://doi.org/10.1007/s11707-018-0707-y, 2019.

Liu, K., Chen, X., Zuza, A., Shao, Z., Qin, X., Han, L., Zhang, Y., Yu, W., Wang, Z., Shi, X., Li, B., and Wang, Y.: The Late Mesozoic Intracontinental contraction-Extension Transition in the Beishan Fold-Thrust Belt, Central Asia: Constraints From Structural Analysis and Apatite (U-Th)/He Thermochronology, TECTONICS, 42, https://doi.org/10.1029/2022TC007532, 2023.

Liu-Zeng, J., Tapponnier, P., Gaudemer, Y., and Ding, L.: Quantifying landscape differences across the Tibetan plateau: Implications for topographic relief evolution, J. Geophys. Res., 113, 2007JF000897, https://doi.org/10.1029/2007JF000897, 2008.

https://doi.org/10.5194/egusphere-2024-3668
Preprint. Discussion started: 17 December 2024

Lu, H. H., Chang, Y. A., Wang, W., and Zhou, Z. Y.: Rapid exhumation of the Tianshan Mountains since the early Miocene: Evidence from combined apatite fission track and (U-Th)/He thermochronology, Sci China Earth Sci, 56, 2116–2125, https://doi.org/10.1007/s11430-013-4715-1, 2013.

Ma, A., Hu, X., Garzanti, E., Han, Z., and Lai, W.: Sedimentary and tectonic evolution of the southern Qiangtang basin: Implications for the Lhasa-Qiangtang collision timing, Journal of Geophysical Research: Solid Earth, 122, 4790–4813, https://doi.org/10.1002/2017JB014211, 2017.

Ma, X. X., Shu, L. S., and Meert, J. G.: Early Permian slab breakoff in the Chinese Tianshan belt inferred from the post-collisional granitoids, Gondwana Res., 27, 228–243, https://doi.org/10.1016/j.gr.2013.09.018, 2015.

Macaulay, E. A., Sobel, E. R., Mikolaichuk, A., Kohn, B., and Stuart, F. M.: Cenozoic deformation and exhumation history of the Central Kyrgyz Tien Shan, Tectonics, 33, 135–165, https://doi.org/10.1002/2013tc003376, 2014.

Meng, Q.-R.: What drove late mesozoic extension of the northern China–mongolia tract?, Tectonophysics, 369, 155–174, https://doi.org/10.1016/S0040-1951(03)00195-1, 2003.

Molnar, P. and Tapponnier, P.: Cenozoic Tectonics of Asia: Effects of a Continental Collision, Science, 189, 419–426, https://doi.org/10.1126/science.189.4201.419, 1975.

Morin, J., Jolivet, M., Barrier, L., Laborde, A., Li, H. B., and Dauteuil, O.: Planation surfaces of the Tian Shan Range (Central Asia): Insight on several 100 million years of topographic evolution, Journal of Asian Earth Sciences, 177, 52–65, https://doi.org/10.1016/j.jseaes.2019.03.011, 2019.

Nachtergaele, S., De Pelsmaeker, E., Glorie, S., Zhimulev, F., Jolivet, M., Danisik, M., Buslov, M. M., and De Grave, J.: Meso-Cenozoic tectonic evolution of the Talas-Fergana region of the Kyrgyz Tien Shan revealed by low-temperature basement and detrital thermochronology, Geoscience Frontiers, 9, 1495–1514, https://doi.org/10.1016/j.gsf.2017.11.007, 2018.

Ni, X., Wang, B., Cluzel, D., Liu, J., and He, Z.: Late paleozoic tectonic evolution of the north tianshan belt: New structural and geochronological constraints from meta-sedimentary rocks and migmatites in the harlik range (NW China), Journal of Asian Earth Sciences, 210, 104711, https://doi.org/10.1016/j.jseaes.2021.104711, 2021.

Pearce, N. J. G., Perkins, W. T., Westgate, J. A., Gorton, M. P., Jackson, S. E., Neal, C. R., and Chenery, S. P.: A Compilation of New and Published Major and Trace Element Data for NIST SRM 610 and NIST SRM 612 Glass Reference Materials, Geostandards Newsletter, 21, 115–144, https://doi.org/10.1111/j.1751-908X.1997.tb00538.x, 1997.

Phillips, J. D.: Erosion, isostatic response, and the missing peneplains, Geomorphology, 45, 225–241, https://doi.org/10.1016/S0169-555x(01)00156-8, 2002.

Pullen, A., Banaszynski, M., Kapp, P., Thomson, S. N., and Cai, F.: A mid-Cretaceous change from fast to slow exhumation of the western Chinese Altai mountains: A climate driven exhumation signal?, Journal of Asian Earth Sciences, 197, 104387, https://doi.org/10.1016/j.jseaes.2020.104387, 2020.

Qin, Y., Liu, C. Y., Yang, L. H., Peng, H., and Jiao, X. Q.: Detrital-Zircon Geochronology of Jurassic-Cretaceous Strata in the Turpan-Hami Basin: Implication for the Late Mesozoic Tectonic Evolution of Eastern Tien Shan, Minerals-Basel, 12, https://doi.org/10.3390/min12080926, 2022.

Rohrmann, A., Kapp, P., Carrapa, B., Reiners, P. W., Guynn, J., Ding, L., and Heizler, M.: Thermochronologic evidence for plateau formation in central Tibet by 45 Ma, Geology, 40, 187–190, https://doi.org/10.1130/G32530.1, 2012.

Rolland, Y., Jourdon, A., Petit, C., Bellahsen, N., Loury, C., Sobel, E. R., and Glodny, J.: Thermochronology of the highest central Asian massifs (Khan Tengri -Pobedi, SE Kyrgyztan): Evidence for Late Miocene (ca. 8 Ma) reactivation of Permian faults and insights into building the Tian Shan, J Asian Earth Sci, 200, https://doi.org/10.1016/j.jseaes.2020.104466, 2020.

https://doi.org/10.5194/egusphere-2024-3668
Preprint. Discussion started: 17 December 2024

Schwab, M., Ratschbacher, L., Siebel, W., McWilliams, M., Minaev, V., Lutkov, V., Chen, F. K., Stanek, K., Nelson, B., Frisch, W., and Wooden, J. L.: Assembly of the Pamirs: Age and origin of magmatic belts from the southern Tien Shan to the southern Pamirs and their relation to Tibet, Tectonics, 23, https://doi.org/10.1029/2003tc001583, 2004.

Shao, L., Stattegger, K., Li, W., and Haupt, B. J.: Depositional style and subsidence history of the Turpan Basin (NW China), Sedimentary Geology, 128, 155–169, https://doi.org/10.1016/S0037-0738(99)00066-4, 1999.

Shao, L., Zhang, P., Hilton, J., Gayer, R., Wang, Y., Zhao, C., and Luo, Z.: Paleoenvironments and paleogeography of the Lower and lower Middle Jurassic coal measures in the Turpan-Hami oil-prone coal basin, northwestern China, AAPG Bulletin, 87, 335–355, https://doi.org/10.1306/09160200936, 2003.

Shen, Chuan. B., Mei, Lian. F., Liu, L., Tang, Ji. G., and Zhou, F.: Evidence from apatite and zircon fission track analysis for Mesozoic-Cenozoic uplift thermal history of Bogeda Mountain of Xinjiang,Northwest China, Marine Geology & Quaternary Geology, 87-92 (in Chinese with English abstract), 2006.

Shen, T., Chen, Y., Wang, G., Ji, J., Wang, Y., Zhang, P., Sotiriou, P., Guo, R., and Xu, Z.: Detrital zircon geochronology analysis of the Late Mesozoic deposition in the Turpan-Hami basin: Implications for the uplift history of the Eastern Tian Shan, north-western China, Terra Nova, 32, 166–178, https://doi.org/10.1111/ter.12445, 2020.

Shen, T., Ding, Y., Wang, G., Zhang, D., and Zhao, Z.: Quaternary deformation along the Gobi–Tian Shan Fault in the Easternmost Tian Shan (Harlik Mountain), Central Asia, Remote Sensing, 16, 3343, https://doi.org/10.3390/rs16173343, 2024.

Sobel, E. R., Oskin, M., Burbank, D., and Mikolaichuk, A.: Exhumation of basement-cored uplifts: Example of the Kyrgyz Range quantified with apatite fission track thermochronology, Tectonics, 25, 17, https://doi.org/10.1029/2005tc001809, 2006a.

Sobel, E. R., Chen, J., and Heermance, R. V.: Late Oligocene-Early Miocene initiation of shortening in the Southwestern Chinese Tian Shan: Implications for Neogene shortening rate variations, Earth and Planetary Science Letters, 247, 70–81, https://doi.org/10.1016/j.epsl.2006.03.048, 2006b.

Song, D. F., Glorie, S., Xiao, W. J., Collins, M. S., Gillespie, J., Jepson, G., and Li, Y. C.: Tectono-thermal evolution of the southwestern Alxa Tectonic Belt, NW China: Constrained by apatite U-Pb and fission track thermochronology, Tectonophysics, 722, 577–594, https://doi.org/10.1016/j.tecto.2017.11.029, 2018.

Song, S. D., Li, J. A., Liu, X. Y., Wang, Y. D., Liang, W. T., and Yuan, S. H.: Mesozoic-Cenozoic Exhumation History of the Bogda Range, Eastern Tianshan: Insights from Apatite Fission Track Thermochronology, Minerals-Basel, 13, https://doi.org/10.3390/min13010071, 2023.

Sui, Q.-L., Wang, Q., Zhu, D.-C., Zhao, Z.-D., Chen, Y., Santosh, M., Hu, Z.-C., Yuan, H.-L., and Mo, X.-X.: Compositional diversity of ca. 110Ma magmatism in the northern Lhasa Terrane, Tibet: Implications for the magmatic origin and crustal growth in a continent–continent collision zone, Lithos, 168–169, 144–159, https://doi.org/10.1016/j.lithos.2013.01.012, 2013.

Sun, J. B., Chen, W., Qin, K. Z., Danisik, M., Evans, N. J., McInnes, B. I. A., Shen, Z., Zhao, S. F., Zhang, B., Yin, J. Y., and Tao, N.: Mesozoic exhumation of the Jueluotage area, Eastern Tianshan, NW China: constraints from (U-Th)/He and fission-track thermochronology, Geol. Mag., 158, 1960–1976, https://doi.org/10.1017/s0016756821000522, 2021.

Sun, Jing. B., Sun, Teng. F., Chen, W., Yu, S., Yin, Ji. Y., Li, C., Zhang, Y., and Liu, Xin. Y.: Thermo-tectonic evolution history of Hongyuntan area, eastern Tianshan, Xinjiang: Constrained from Ar-Ar and (U-Th)/He dating, Acta Petrologica Sinica, 31, 3732-3742 (in Chinese with English abstract), 2015.

Suo, Y. H., Li, S. Z., Cao, X. Z., Dong, H., Li, X. Y., and Wang, X. Y.: Two-stage eastward diachronous model of India-Eurasia collision: Con-straints from the intraplate tectonic records in Northeast Indian Ocean, GONDWANA RESEARCH, 102, 372–384, https://doi.org/10.1016/j.gr.2020.01.006, 2022.

https://doi.org/10.5194/egusphere-2024-3668
Preprint. Discussion started: 17 December 2024

Tang, W., Zhang, Z., Li, J., and Chen, C.: Geochemical characteristics and tectonic significance of the Cretaceous volcanic rocks in the Eastern Terminal of the Altyn Tagh fault zones, Earth Science Frontiers, 19, 51–62, 2012.

Tang, W. H., Zhang, Z. C., Li, J. F., Li, K., Luo, Z. W., and Chen, Y.: Mesozoic and Cenozoic uplift and exhumation of the Bogda Mountain, NW China: Evidence from apatite fission track analysis, Geosci. Front., 6, 617–625, https://doi.org/10.1016/j.gsf.2014.04.006, 2015.

Tian, Z., Xiao, W., Zhang, Z., and Lin, X.: Fisson-track constrains on superposed folding in the Beishan orogenic belt, southernmost Altaids, Geoscience Frontiers, 7, 181–196, https://doi.org/10.1016/j.gsf.2015.11.007, 2016.

van der Beek, P. A., Delvaux, D., Andriessen, P. A. M., and Levi, K. G.: Early Cretaceous denudation related to convergent tectonics in the Baikal region, SE Siberia. Journal of the Geological Society, 153, 515–523, 1996.

van der Beek, P., Van Melle, J., Guillot, S., Pêcher, A., Reiners, P. W., Nicolescu, S., and Latif, M.: Eocene Tibetan plateau remnants preserved in the northwest Himalaya, Nature Geosci, 2, 364–368, https://doi.org/10.1038/ngeo503, 2009.

van Hinsbergen, D. J. J., Lippert, P. C., Dupont-Nivet, G., McQuarrie, N., Doubrovine, P. V., Spakman, W., and Torsvik, T. H.: Greater India Basin hypothesis and a two-stage Cenozoic collision between India and Asia, P Natl Acad Sci USA, 109, 7659–7664, https://doi.org/10.1073/pnas.1117262109, 2012.

Vermeesch, P.: RadialPlotter: A Java application for fission track, luminescence and other radial plots, Radiation Measurements, 44, 409–410, https://doi.org/10.1016/j.radmeas.2009.05.003, 2009.

Vermeesch, P.: Statistics for LA-ICP-MS based fission track dating, Chem. Geol., 456, 19–27, https://doi.org/10.1016/j.chemgeo.2017.03.002, 2017.

Vermeesch, P.: Statistics for Fission-Track Thermochronology, in: Fission-Track Thermochronology and its Application to Geology, edited by: Malusà, M. G. and Fitzgerald, P. G., Springer International Publishing, Cham, 109–122, https://doi.org/10.1007/978-3-319-89421-8_6, 2019.

Wang, F., Luo, M., He, Z., Wang, Y., Zheng, B., Zhang, Z., Hu, X., and Zhu, W.: Mid-Cretaceous Accelerated Cooling of the Beishan Orogen, NW China: Evidence from Apatite Fission Track Thermochronology, Lithosphere, 2023, lithosphere_2023_239, https://doi.org/10.2113/2023/lithosphere_2023_239, 2024.

Wang, G., Cao, K., Zhang, K., Wang, A., Liu, C., Meng, Y., and Xu, Y.: Spatio-temporal framework of tectonic uplift stages of the Tibetan Plateau in Cenozoic, Sci. China Earth Sci., 54, 29–44, https://doi.org/10.1007/s11430-010-4110-0, 2011.

Wang, Q. C., Li, S. J., and Du, Z. L.: Differential uplift of the Chinese Tianshan since the Cretaceous: constraints from sedimentary petrography and apatite fission-track dating, Int J Earth Sci, 98, 1341–1363, https://doi.org/10.1007/s00531-009-0436-2, 2009.

Wang, T., Guo, L., Zhang, L., Yang, Q., Zhang, J., Tong, Y., and Ye, K.: Timing and evolution of Jurassic–Cretaceous granitoid magmatisms in the Mongol–Okhotsk belt and adjacent areas, NE Asia: Implications for transition from contractional crustal thickening to extensional thinning and geodynamic settings, Journal of Asian Earth Sciences, 97, 365–392, https://doi.org/10.1016/j.jseaes.2014.10.005, 2015.

Wang, T., Tong, Y., Xiao, W., Guo, L., Windley, B. F., Donskaya, T., Li, S., Tserendash, N., and Zhang, J.: Rollback, scissor-like closure of the Mongol-Okhotsk Ocean and formation of an orocline: magmatic migration based on a large archive of age data, National Science Review, 9, nwab210, https://doi.org/10.1093/nsr/nwab210, 2022.

Wang, X., Kellner, A. W. A., Jiang, S., Cheng, X., Wang, Q., Ma, Y., Paidoula, Y., Rodrigues, T., Chen, H., Sayão, J. M., Li, N., Zhang, J., Bantim, R. A. M., Meng, X., Zhang, X., Qiu, R., and Zhou, Z.: Egg accumulation with 3D embryos provides insight into the life history of a pterosaur, Science, 358, 1197–1201, https://doi.org/10.1126/science.aan2329, 2017.

Wang, Y., Wang, Y., Yin, J., Thomson, S. N., Xiao, W., He, Z., Chen, W., Cai, K., Wu, M., and Meng, Y.: Mesozoic exhumation of the northern west junggar, NW China: Insights from low-temperature thermochronometers, Tectonophysics, 862, 229939, https://doi.org/10.1016/j.tecto.2023.229939, 2023a.

https://doi.org/10.5194/egusphere-2024-3668
Preprint. Discussion started: 17 December 2024

Wang, Y. N., Cai, K. D., Sun, M., Xiao, W. J., De Grave, J., Wan, B., and Bao, Z. H.: Tracking the multi-stage exhumation history of the western Chinese Tianshan by apatite fission track (AFT) dating: Implication for the preservation of epithermal deposits in the ancient orogenic belt, Ore Geology Reviews, 100, 111–132, https://doi.org/10.1016/j.oregeorev.2017.04.011, 2018.

Wang, Y. N., Zhang, J., Huang, X., and Wang, Z. J.: Cenozoic exhumation of the Tianshan as constrained by regional low-temperature thermochronology, Earth-Sci. Rev., 237, 24, https://doi.org/10.1016/j.earscirev.2023.104325, 2023b.

Whipple, K. X., DiBiase, R. A., Ouimet, W. B., and Forte, A. M.: Preservation or piracy: Diagnosing low-relief, high-elevation surface formation mechanisms, Geology, 45, 91–94, https://doi.org/10.1130/G38490.1, 2017.

Windley, B. F., Allen, M. B., Zhang, C., Zhao, Z. Y., and Wang, G. R.: Paleozoic Accretion and Cenozoic Redeformation of the Chinese Tien-Shan-Range, Central-Asia, Geology, 18, 128–131, https://doi.org/10.1130/0091-7613(1990)018<0128:Paacro>2.3.Co;2, 1990.

Windley, B. F., Alexeiev, D., Xiao, W. J., Kroner, A., and Badarch, G.: Tectonic models for accretion of the Central Asian Orogenic Belt, J. Geol. Soc., 164, 31–47, https://doi.org/10.1144/0016-76492006-022, 2007.

Wu, H., Li, C., Hu, P., and Li, X.: Early Cretaceous (100–105 Ma) Adakitic magmatism in the Dachagou area, northern Lhasa terrane, Tibet: implications for the Bangong–Nujiang Ocean subduction and slab break-off, International Geology Review, 57, 1172–1188, https://doi.org/10.1080/00206814.2014.886152, 2015.

Wu, M., Yin, J., He, Z., Xiao, W., Wang, Y., Chen, W., Wang, Y., Sun, J., Li, D., and Meng, Y.: Mesozoic Thermo-Tectonic Evolution of the Western Altai Orogenic Belt (NW China): Insights from Low-Temperature Thermochronology, Lithosphere, 2023, 8161000, https://doi.org/10.2113/2023/8161000, 2023.

Xiang, D. F., Zhang, Z. Y., Xiao, W. J., Zhu, W. B., Zheng, D. W., Li, G. W., Zheng, B. H., Song, D. F., Han, C. M., and Pang, J. Z.: Episodic Meso-Cenozoic denudation of Chinese Tianshan: evidence from detrital apatite fission track and zircon U-Pb data, southern Junggar Basin margin, NW China, Journal of Asian Earth Sciences, 175, 199–212, https://doi.org/10.1016/j.jseaes.2018.07.042, 2019.

Xiao, W. J., Zhang, L. C., Qin, K. Z., Sun, S., and Li, J. L.: Paleozoic accretionary and collisional tectonics of the Eastern Tianshan (China): Implications for the continental growth of Central Asia, Am. J. Sci., 304, 370–395, https://doi.org/10.2475/ajs.304.4.370, 2004.

Xiao, W. J., Windley, B. F., Allen, M. B., and Han, C. M.: Paleozoic multiple accretionary and collisional tectonics of the Chinese Tianshan orogenic collage, Gondwana Research, 23, 1316–1341, https://doi.org/10.1016/j.gr.2012.01.012, 2013.

Yang, R., Willett, S. D., and Goren, L.: In situ low-relief landscape formation as a result of river network disruption, Nature, 520, 526–529, https://doi.org/10.1038/nature14354, 2015a.

Yang, Y. T., Guo, Z. X., Song, C. C., Li, X. B., and He, S.: A short-lived but significant Mongol-Okhotsk collisional orogeny in latest Jurassic-earliest Cretaceous, Gondwana Res, 28, 1096–1116, https://doi.org/10.1016/j.gr.2014.09.010, 2015b.

Yin, A. and Harrison, T. M.: Geologic Evolution of the Himalayan-Tibetan Orogen, Annu. Rev. Earth Planet. Sci., 28, 211–280, https://doi.org/10.1146/annurev.earth.28.1.211, 2000.

Yin, J. Y., Chen, W., Hodges, K. V., Xiao, W. J., Cai, K. D., Yuan, C., Sun, M., Liu, L. P., and van Soest, M. C.: The thermal evolution of Chinese central Tianshan and its implications: Insights from multi-method chronometry, Tectonophysics, 722, 536–548, https://doi.org/10.1016/j.tecto.2017.11.037, 2018.

Yuan, J., Yang, Z., Deng, C., Krijgsman, W., Hu, X., Li, S., Shen, Z., Qin, H., An, W., He, H., Ding, L., Guo, Z., and Zhu, R.: Rapid drift of the Tethyan Himalaya terrane before two-stage India-Asia collision, National Science Review, 8, nwaa173, https://doi.org/10.1093/nsr/nwaa173, 2021.

Zhang, B., Yang, J., Yang, L., Chen, H., Liu, J., Wang, F., and Wu, L.: Mesozoic-Cenozoic Exhumation Processes of the Harlik Mountain (East Tianshan), NW China: Evidence from Apatite (U-Th)/He Thermochronology, Lithosphere, 2023, lithosphere_2023_210, https://doi.org/10.2113/2023/lithosphere_2023_210, 2023.

https://doi.org/10.5194/egusphere-2024-3668
Preprint. Discussion started: 17 December 2024

Zhang, D., Wang, G., Pullen, A., Abell, J. T., Cheng, F., Shen, T., Ji, J., and Zhang, M.: A westerly dominated Early Cretaceous eolian system in the Hami Basin, NW China, Geological Society of America Bulletin, https://doi.org/10.1130/B37436.1, 2024.

Zhang, W., Chen, W., Sun, J. B., Shen, Z., and Zhang, Y.: Thermal history and exhumation processes in the Chinese South Tianshan: constraints from Ar-40/Ar-39 and (U-Th)/He ages, Int. J. Earth Sci., 18, https://doi.org/10.1007/s00531-021-02031-x, 2021.

Zhang, Z. Y., Zhu, W. B., Shu, L. S., Wan, J. L., Yang, W., Su, J. B., and Zheng, B. H.: Apatite fission track thermochronology of the Precambrian Aksu blueschist, NW China: Implications for thermo-tectonic evolution of the north Tarim basement, Gondwana Research, 16, 182–188, https://doi.org/10.1016/j.gr.2009.04.006, 2009.

Zhang, Z. Y., Zhu, W. B., Shu, L. S., Wan, J. L., Yang, W., Zheng, B. H., and Su, J. B.: Multi-stage exhumation of the NE Tarim Precambrian bedrock, NW China: constraints from apatite fission track thermochronology in the Kuluketage area, Terra Nova, 23, 324–332, https://doi.org/10.1111/j.1365-3121.2011.01017.x, 2011.

Zhang, Z. Y., Zhu, W. B., Zheng, D. W., Zheng, B. H., and Yang, W.: Apatite fission track thermochronology in the Kuluketage and Aksu areas, NW China: Implication for tectonic evolution of the northern Tarim, Geosci Front, 7, 171–180, https://doi.org/10.1016/j.gsf.2015.08.007, 2016.

Zheng, D., Chang, S.-C., Ramezani, J., Xu, X., Xu, H., Wang, H., Pei, R., Fang, Y., Wang, J., Wang, B., and Zhang, H.: Calibrating the Early Cretaceous Urho Pterosaur Fauna in Junggar Basin and implications for the evolution of the Jehol Biota, GSA Bulletin, 136, 765–773, https://doi.org/10.1130/B36795.1, 2023.

Zhimulev, F. I., Vetrov, E. V., Novikov, I. S., Van Ranst, G., Nachtergaele, S., Dokashenko, S. A., and De Grave, J.: Mesozoic Intracontinental Orogeny in the Tectonic History of the Kolyvan'- Tomsk Folded Zone (Southern Siberia): a Synthesis of Geological Data and results of Apatite Fission Track Analysis, Russ. Geol. Geophys., 62, 1006–1020, https://doi.org/10.2113/rgg20204172, 2021.

Zhu, W., Shu, L., Wan, J., Sun, Y., Wang, F., and Zhao, Z.: Fission-track Evidence for the Exhumation History of Bogda-Harlik Mountains, Xinjiang Since the Cretaceous, Acta Geologica Sinica, 16-22 (in Chinese with English abstract), 2006.

Zhu, W. B., Wan, J. L., Shu, L. S., Sun, Y., and Wang, F.: Mesozoic-Cenozoic thermal history of Turpan-Hami basin: evidence from apatite fission track, Progress in Naturalence, 14, 1194-1198 (in Chinese with English abstract), https://doi.org/10.3321/j.issn:1002-008X.2004.10.017, 2004.

Zhu, Wen. B., Zhang, Z., Shu, L., Wan, J., Lu, H., Wang, S., Yang, W., and Su, J.: Uplift and exhumation history of the Precambrian basement, Northern Tarim: Evidence from apatite fission track data, Acta Petrologica Sinica, 23, 1671-1682 (in Chinese with English abstract), https://doi.org/10.3969/j.issn.1000-0569.2007.07.013, 2007.